AN ABSTRACT OF THE THESIS OF

Katja Münzenmayer for the degree of Master of Arts in Mathematics presented on July 27, 1993.

Title: The Fractal Structure of Surface Water Waves near Breaking

Redacted for privacy

Abstract approved: _____

Ronald B. Guenther

The goal of this research project is to determine the fractal nature, if any, which certain surface water waves exhibit when viewed on a microscopic scale. We make use of the mathematical formulation of non-viscous fluids describing their physical properties. Using these expressions and including boundary conditions for free surfaces as well as taking the surface tension into consideration, we obtain a partial differential equation describing the dynamics of surface water waves.

A brief introduction to the study of fractal geometry with several examples of well-known fractals is included. An important property of fractals is their non-integral dimension. Several methods of determining the dimension of a curve are described in this paper.

Our wave equation is examined under different assumptions representing the conditions of a surface water wave near its breaking point. Solutions are developed using analytical and numerical methods. We determine the dimension of 'rough' solutions using one of the methods introduced and conclude that under certain conditions, surface water waves near their breaking point exhibit a fractal structure on a microscopic scale.

The Fractal Structure of Surface Water Waves near Breaking

by

Katja Münzenmayer

A THESIS
submitted to
Oregon State University

in partial fulfillment of the
requirements for the degree of

Master of Arts

Completed July 27, 1993
Commencement June 1994

Für meine Eltern

... there is a God precisely because Nature itself, even in chaos, cannot proceed except in an orderly and regular manner.

Immanuel Kant

Approved:

Redacted for privacy

Professor of Mathematics in charge of major

Redacted for privacy

Head of Department of Mathematics

Redacted for privacy

Dean of Graduate School

Date thesis is presented: July 27, 1993

ACKNOWLEDGEMENTS

This project would not have been completed without the support and encouragement of many people.

Thanks go first and foremost to Dr. Ronald B. Guenther for guiding and directing this research. He has greatly aided my understanding of mathematics. The careful attention and interest he showed in my work as well as the enthusiasm he shared with me were essential for both the beginning and completion of this project.

Prof. Andre Weideman has been most generous with his time in helping with the numerical analysis.

The advice and help of fellow students, in particular Isa Jubran, and staff members at the Department of Mathematics for saving me countless hours of computer- and language-related problems is gratefully appreciated.

Table of Contents

Table of Contents (Cont.)

List of Figures

List of Figures (Cont.)

List of Tables

The Fractal Structure of Surface Water Waves near Breaking

Chapter 1

Introduction

The study of *fractals* and *chaotic systems* is a fairly recent topic in the field of mathematics. Great mathematicians of the past: Karl Weierstrass, Georg Cantor, Guiseppe Peano, David Hilbert, Helge von Koch, Waclaw Sierpinski, Gaston Julia and Felix Hausdorff to name a few, already considered ideas that are now related to the notion of fractals. However, fractals were regarded as exceptional objects or 'mathematical monsters' until quite recently, see [Peit, 1992]. Despite this early development, *fractal geometry* did not become popular until after the sixties when Benoit B. Mandelbrot founded this new branch of mathematics. It did not happen earlier partly due to philosophical reasons (people were convinced that natural processes were smooth), and partly because technology was not sufficiently advanced (the early computers were not powerful enough to carry out the numerically intensive calculations necessary to compute fractal structures). Tech-

nological developments have made it possible to discover the beauty and fascination of fractals.

The typical way in which we visualize a fractal is as a complex, geometrical pattern. Despite its complexity, it is surprising that the mathematical equations behind it are usually very simple. This phenomenon of complexity resulting from simplicity is common throughout fractal geometry and chaos theory.

Some of the computer images of fractals resemble patterns arising in nature and therefore encouraged the task of finding fractal images which look 'natural'. Success in this area is another reason why fractals are so fascinating. One realized that, for instance, ferns, trees, coast lines, clouds and mountains possess a fractal structure.

The problem of bringing order into chaos is an age old human endeavor. Johannes Kepler attempted to model our solar system and discovered for himself the complexity involved in such a task.

The study of chaotic patterns is part of the field of 'strongly' nonlinear systems or systems far from equilibrium. In physics, one such 'strongly' nonlinear system is a fluid in turbulent motion. Although we might not find chaotic systems in all problems that contain fluids in turbulent motion, the presence of it strongly suggests that we examine the problem from the fractal perspective. In this thesis we will consider surface water waves just before they break and show that they exhibit a fractal structure.

The notion of *fractal structure* we use here is not equivalent to *self-similarity*

(which is used for Cantor sets, von Koch curves and Julia sets), but rather describes *roughness*. A 'rough' surface will not be of dimension 2 as any other 'usual' (or smooth) surface would be, but rather of a non-integer dimension between 2 and 3. A sufficient condition for a set to be a fractal is for it to have a non-integer dimension. Several ways of finding the dimension of curves or areas will be described in this paper.

The *fractal objects* we investigate in this thesis are surface water waves. To describe the dynamics of waves mathematically, one begins with the basic equations of fluid dynamics of non-viscous fluids. Very often when the behavior of water waves is considered, the condition of surface tension is excluded. In this thesis, while making other customary simplifications, we shall include the condition of surface tension. Under the boundary conditions of free surfaces, we shall reach a differential equation that represents the dynamics of breaking surface water waves. In order to analyze this equation, we will break it up into multiple cases according to different physical conditions. Then with the sine curve as the initial condition, we shall show that the solutions for some of these cases develop into highly irregular, non-differentiable curves. The fractal dimension of these curves leads to the conclusion that, under certain conditions, surface water waves possess a fractal surface structure.

The present thesis is divided in four parts:

1. Chapter 2 describes the basic notions and mathematical descriptions of water waves.

2. Chapter 3 presents the basic ideas and definitions of fractals, along with a discussion of several well-known fractals that promote understanding of the notion 'fractal'. Furthermore, we introduce several ways of determining the fractal dimension of a set.

3. The results of Chapter 2 are analyzed in Chapter 4 under different conditions. We shall obtain several equations which will be solved either analytically or numerically and are then simulated. Two of these cases possess a rough surface.

4. In the last part, one of these rough surfaces will be determined to be fractal by using the methods introduced in chapter 3 of finding the fractal dimension.

Chapter 2

Waves

There exist two principle ways to describe continuum processes. One uses the Lagrangian, the other one the Eulerian approach. Lagrange's method is based on four independent variables, which are time t and the spatial variables x_0, y_0, z_0 of a particle in a reference position, e.g. position at time $t = 0$. The position as well as the pressure and density at time t are described using the paths of individual fluid particles in reference to the position x_0, y_0 and z_0. This method is useful if one wants to study the characteristic properties of solid bodies. In Euler's method, the four independent variables are time t and the spatial coordinates x, y, z. One uses the velocity (and acceleration) field in the region occupied by a fluid at a given moment, to describe the velocity v, pressure p and density ρ, which will then be functions of x, y, z and t. In our case, the Eulerian approach is much more applicable.

For notational convenience, we shall write a variable $x = (x_1, x_2, x_3)$, if it is clear from the context that we talk about three dimensions.

2.1 Conservation of Mass

The mass m of a fluid that occupies a volume V is given by the formula

$$m = \int_V \varrho \, dx, \tag{2.1}$$

where $\varrho = \varrho(x,t), \varrho > 0$ is the density of the fluid.

The principle of conservation of mass states:

The mass of a fluid in a material volume V does not change as V moves with the fluid,

or alternatively:

The rate of change of mass in a fixed volume V is equal to the mass flux through its surface,

which is expressed by the following equation:

$$\frac{d}{dt}\int_V \varrho \, dx = -\int_S \varrho(v \cdot n) dS.$$

Using the divergence theorem, we get:

$$\int_V \varrho_t \, dx = -\int_V \operatorname{div}(\varrho v) dx$$

$$\int_V [\varrho_t + \operatorname{div}(\varrho v)] dx = 0.$$

Since V is arbitrary,

$$\varrho_t + \operatorname{div}(\varrho v) = 0. \tag{2.2}$$

2.2 Navier-Stokes' Equations

The totality of the forces that act on a fluid are pressure, gravity and friction. We get the equation:

$$\varrho a = -\nabla p - \varrho g + \mu \Delta v, \tag{2.3}$$

where p is pressure, g is the acceleration of gravity, ϱ is density, μ is viscosity and a is acceleration.

To get an explicit formula for the acceleration a, we first calculate the coordinates of a:

$$a = \frac{dv}{dt}$$

$$\begin{aligned} \frac{dv_i}{dt} &= \frac{\partial v_i}{\partial t} + \frac{\partial v_i dx}{\partial x dt} + \frac{\partial v_i dy}{\partial y dt} + \frac{\partial v_i dz}{\partial z dt} \\ &= \frac{\partial v_i}{\partial t} + \frac{\partial v_i}{\partial x} v_1 + \frac{\partial v_i}{\partial y} v_2 + \frac{\partial v_i}{\partial z} v_3 \\ &= \frac{\partial v_i}{\partial t} + (v\nabla) v_i \\ \Rightarrow a &= \frac{dv}{dt} = \frac{\partial v}{\partial t} + (v\nabla)v = \frac{\partial v}{\partial t} + \nabla \frac{|v|^2}{2} + \mathrm{rot} v \times v. \end{aligned} \tag{2.4}$$

Inserting this in equation (2.3), we get the important **Navier-Stokes' equations** in the form:

$$\varrho \frac{\partial v}{\partial t} + \varrho (v\nabla)v = -\nabla p - \varrho g + \mu \Delta v. \tag{2.5}$$

The fluid may have specific properties, which lead to further conditions:

- inviscid fluid $\Rightarrow \mu = 0$.

  An inviscid fluid is also called an 'ideal' fluid. The Navier-Stokes' equations

reduce to the **Euler equations**:

$$\varrho\frac{\partial v}{\partial t} + \varrho(v\nabla)v = -\nabla p - \varrho g.$$

- incompressible fluid $\Rightarrow \varrho = \text{const.}$

  Equation (2.2) implies now, that

$$\text{div}v = 0, \tag{2.6}$$

  which is known as the *continuity condition.*

- irrotationality $\Rightarrow \text{rot}v = 0.$

  An irrotational fluid is always inviscid. Equation (2.4) and equation (2.5) imply therefore:

$$\varrho\frac{\partial v}{\partial t} + \varrho\nabla\frac{|v|^2}{2} = -\nabla p - \varrho g. \tag{2.7}$$

The rotation of v being zero in a closed region Ω implies that there exists a function $\varphi : \Omega \to \mathbf{R}$ such that $\nabla\varphi = v$, where φ is called the *velocity potential.* Using this in equation (2.7), we get:

$$\varrho\frac{\partial(\nabla\varphi)}{\partial t} + \varrho\nabla\frac{|\nabla\varphi|^2}{2} = -\nabla p - \varrho g.$$

Since the gravitational acceleration has only a component in the z-direction, we note that $\varrho g = \nabla(\varrho g z)$, and hence:

$$\nabla(\varrho\frac{\partial\varphi}{\partial t} + \varrho\frac{|\nabla\varphi|^2}{2} + p + \varrho g z) = 0$$

$$\varrho\frac{\partial\varphi}{\partial t} + \varrho\frac{|\nabla\varphi|^2}{2} + p + \varrho g z = c, \tag{2.8}$$

where c is an arbitrary function of t.

This equation is called **Bernoulli equation**. $c(t)$ can be taken to equal zero, since we can always replace φ by $\psi + \varrho^{-1} \int_0^t c(\tau)d\tau$ in calculating velocities. If we use $\nabla\varphi = v$ in equation (2.6), we obtain the well-known **Laplace equation**:

$$\Delta\varphi = 0.$$

2.3 Boundary Conditions at a Free Surface

Let $z = h(x, y, t)$ describe the surface $S(t)$. We assume $|\nabla h|^2 \neq 0$. The surface must satisfy several conditions: The velocity of a point (x, y, z) on the surface in the direction of the surface normal is given by:

$$-\frac{h_t}{({h_x}^2 + {h_y}^2 + {h_z}^2)^{\frac{1}{2}}}.$$

A particle of fluid at the same point of the surface at that instant has a velocity component in the direction of the surface normal given by:

$$v_n = \frac{uh_x + vh_y + wh_z}{({h_x}^2 + {h_y}^2 + {h_z}^2)^{\frac{1}{2}}}.$$

Since $S(t)$ is a boundary surface, there can be no transfer of matter across the surface, which motivates the equation

$$0 = \frac{dh}{dt} = h_t + uh_x + vh_y + wh_z.$$

The last equation implies the following:

$$uh_x + vh_y + wh_z = -h_t.$$

In addition to the above, there are further dynamical conditions to be satisfied at a surface. Considering a fluid with surface tension, we have to assume the following: The effect of surface tension as one passes through the interface is to produce a discontinuity in the normal stress proportional to the mean curvature κ of the boundary surface:

$$[p] = \sigma\kappa, \tag{2.9}$$

where σ is a constant. In the case of two-dimensional motion, the curvature is given by:

$$\kappa = \frac{h_{xx}}{(1+h_x^2)^{3/2}}.$$

2.4 Mathematical Description of a Wave

The kinetic energy of a water volume is described by the following integral:

$$E_{kin} = \frac{1}{2}\varrho \int_{V(t)} |\nabla\varphi|^2 dx, \tag{2.10}$$

where φ is the velocity potential introduced in section 2.2 for an irrotational fluid. Taking the derivative of equation (2.10), we find:

$$\begin{aligned} \frac{d}{dt}E_{kin} &= \frac{d}{dt}\left(\frac{1}{2}\varrho \int_{V(t)} |\nabla\varphi|^2 dx\right) \\ &= \varrho \int_{V(t)} \nabla\varphi\nabla\varphi_t dx + \frac{1}{2}\varrho \int_{S(t)} |\nabla\varphi|^2 \frac{\partial\varphi}{\partial n} dS. \end{aligned} \tag{2.11}$$

The first integral in (2.11) can be transformed using Green's identity:

$$\int_V u\Delta w + \int_V \nabla u\nabla w = \int_S u\frac{\partial w}{\partial n}.$$

Therefore, we obtain:

$$\frac{d}{dt}E_{kin} = -\varrho \int_{V(t)} \varphi_t \Delta\varphi dx + \varrho \int_{S(t)} \varphi_t \frac{\partial\varphi}{\partial n} dS + \frac{1}{2}\varrho \int_{S(t)} |\nabla\varphi|^2 \frac{\partial\varphi}{\partial n} dS.$$

Since water can be assumed to be irrotational and incompressible, $\Delta\varphi = 0$ and we obtain:

$$\frac{d}{dt}E_{kin} = \varrho \int_{S(t)} \left(\varphi_t + \frac{1}{2}|\nabla\varphi|^2\right) \frac{\partial\varphi}{\partial n} dS. \tag{2.12}$$

The Bernoulli equation (2.8) and equation (2.12) imply therefore:

$$\frac{d}{dt}E_{kin} = \varrho \int_{S(t)} \left(\varphi_t + \frac{1}{2}|\nabla\varphi|^2\right) \frac{\partial\varphi}{\partial n} dS \tag{2.13}$$

$$= -\int_{S(t)} (p + \varrho g h) \frac{\partial\varphi}{\partial n} dS. \tag{2.14}$$

The above equation is true for the surface of any volume element, so it is also true for the water surface. At the interface of water and air, the pressure p becomes the pressure difference $[p]$ of water pressure p_w and air pressure p_a. The air pressure is approximately zero. Therefore $[p] = p_w$. At the water surface, we have the equality of water pressure and surface tension. Combining the equation for surface tension (2.9) and equation (2.14), we get:

$$\frac{d}{dt}E_{kin} = \int_{S(t)} (\sigma\kappa - \varrho g h) \frac{\partial\varphi}{\partial n} dS. \tag{2.15}$$

If we consider now the time derivative of the work W, we find $\frac{dW}{dt} = F \cdot$ velocity. The velocity is the time derivative of $h(x(t), t)$, therefore we obtain:

$$\frac{d}{dt}h(x(t), t) = h_t + \frac{\partial h}{\partial x}\frac{dx}{dt} = h_t + v_1 h_x,$$

where $v_1 = \frac{dx}{dt}$. The derivative $\frac{dx}{dt}$ is the drift in the x-direction which we set equal to νh. Using this result, we find that the derivative of work is represented by the following:

$$\begin{aligned} \frac{dW}{dt} &= F \cdot \text{velocity} \\ &= F\left(h_t + \nu h h_x\right) \\ &= \int_{S(t)} \lambda\left(h_t + \nu h h_x\right) \frac{\partial \varphi}{\partial n} dS. \end{aligned} \tag{2.16}$$

Conservation of energy implies that the time derivatives of the kinetic energy and the work have to be equal:

$$\int_{S(t)} \left(\sigma\kappa - \varrho g h\right) \frac{\partial \varphi}{\partial n} dS = \int_{S(t)} \lambda\left(h_t + \nu h h_x\right) \frac{\partial \varphi}{\partial n} dS. \tag{2.17}$$

This equality holds for every surface, therefore we have to have equality of the coefficients of $\frac{\partial \varphi}{\partial n}$ and obtain:

$$\sigma\kappa - \varrho g h = \lambda\left(h_t + \nu h h_x\right).$$

Division by λ gives us the general equation:

$$h_t + \nu h h_x = \sigma_1 \kappa - \varrho_1 g h,$$

which alters in two dimensions to:

$$h_t + \nu h h_x = \sigma_1 \frac{h_{xx}}{(1 + h_x^2)^{3/2}} - \varrho_1 g h. \tag{2.18}$$

In order to give a mathematical description of a wave, we used a plausibility argument. The rigorous derivation of equation (2.18) is a statistical argument at a microscopic level which is then averaged. One can find discussions of the strict derivations in [Krug, 1991], [Baus, 1981], [Wall, 1979], [Kawa, 1982-1], [Kawa, 1982-2],

[Buff, 1965] and [Dieh, 1980]. Our derivation was not given at a microscopic level, rather at a macroscopic, to promote understanding and give a motivation why the equation is true.

Chapter 3

Fractals

The word *fractal* was first introduced by Benoit B. Mandelbrot in his fundamental essay: *Fractals and turbulence: attractors and dispersion* [Mand, 1977a]. It is derived from the Latin 'fractus' (meaning 'broken') to describe objects that were too irregular to fit into a traditional geometric setting. Since then many different definitions of fractals have been used. The characteristic properties of fractals we are considering are the following.

Properties: Let the set F be a fractal. Then

- F has a fine structure, i.e. detail on arbitrarily small scales.
- F is too irregular to be described in traditional geometrical language, both locally and globally, i.e. near each of its points are a large number of other points, separated by gaps of varying length.
- Many fractals have some degree of self-similarity, either approximate or statistical.

- Classical geometry or calculus cannot be used to describe fractals, so one has to find alternative techniques. One of these techniques is to find the fractal dimension, which can be defined in several different ways, as one can see in section 3.2.

- Usually the *fractal dimension* of F (defined in some way) is greater than its topological dimension. This means that the size of F is not quantified by the usual measures, such as length.

- In most cases of interest, F is defined in a recursive manner, although it has an intricate detailed structure.

We will now focus on the construction of some examples of fractal sets and prove for some of them why they are considered to be a fractal set.

3.1 Examples of Fractals

3.1.1 The Cantor Set

The most important 'early' fractal is the *Cantor set*, which is also known as the Cantor dust, the Cantor space or the Cantor discontinuum. Georg Cantor (1845-1918), a German mathematician at the University of Halle, first published his set in 1883. The set is visually less appealing than most other fractal sets, and being so peculiar and pathological, it is taken for granted that it cannot be used for any immediate natural interpretation. The basic middle third Cantor set is the

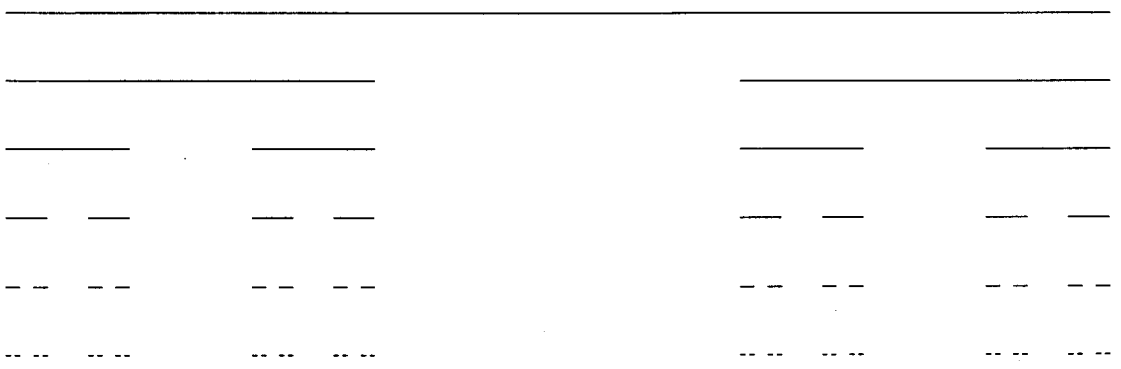

Figure 1. Initial steps of the construction of the Cantor set.

infinite number of points in [0,1], which have a base-3 expansion $x = \sum a_j 3^{-j}$ with $a_j = 0$ or 2 for all j. Therefore the set contains the following numbers:

$$0,\ 1,\ 1/3,\ 2/3,\ 1/9,\ 2/9,\ 7/9,\ 8/9,\ \ldots$$

The classical construction that makes it easier to imagine the set is shown in figure 1. We start with the interval [0, 1] and take away the open (middle third) interval (1/3, 2/3). The next step will take away the middle third of the two remaining closed intervals. In the following step we remove the middle thirds of the now four remaining intervals. The Cantor set is the set of points that remains after doing the procedure of removing the middle third infinitely often. The endpoints of all the closed intervals that appear throughout the construction are elements of the Cantor set.

3.1.2 The Von-Koch Curve

Helge von Koch, a Swedish mathematician, introduced in 1904 what is now called the *von-Koch curve*. The geometric construction can be seen in figures 2, 3, 4 and 5.

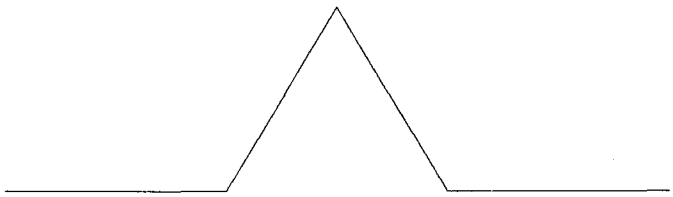

Figure 2. First step of the construction of the von-Koch curve.

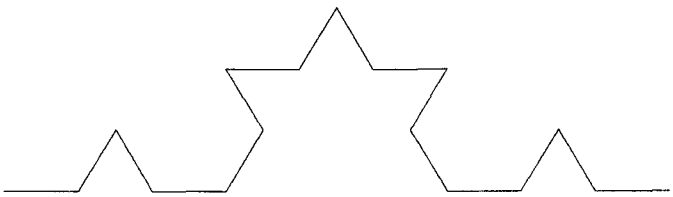

Figure 3. Second step of the construction of the von-Koch curve.

As with the Cantor set, the von-Koch curve is also constructed recursively. We start with a straight line, partition it into three equal parts, then replace the middle part by an equilateral triangle and take away its base. The von-Koch curve is the curve that is obtained after doing this construction step infinitely often. The curve is everywhere continuous, but nowhere differentiable. It contains no straight lines or segments which are smooth. The complexity of the curve reminds much more of

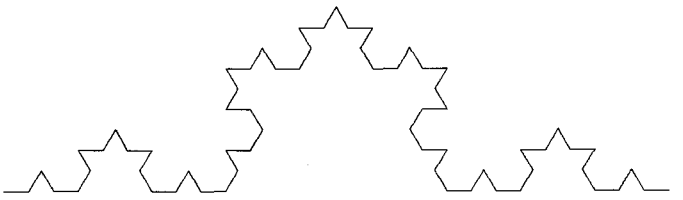

Figure 4. Third step of the construction of the von-Koch curve.

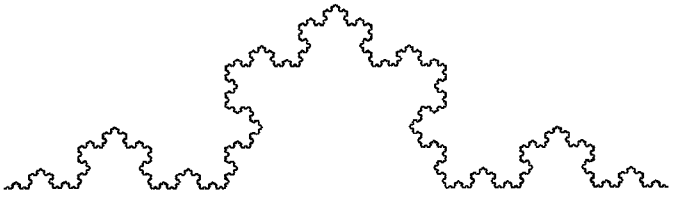

Figure 5. Seventh step of the construction of the von-Koch curve.

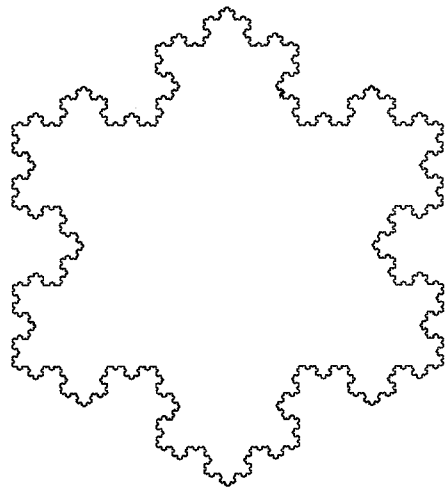

Figure 6. The snowflake curve obtained from three von-Koch curves.

the complexity one would see in a natural coastline, folds within folds within folds. Fitting together three suitably rotated copies of the von-Koch curve produces the so-called snowflake curve or the Koch island, which is shown in figure 6.

3.1.3 Julia and Mandelbrot Sets

Much of the theory of *Julia sets* was developed at the beginning of the twentieth century by the French mathematician Gaston Julia. Since, in this time, he did not have the tools of modern technology, his results did not seem and especially look as impressive as they do today, when the sets are made visible with the help of a computer. Benoit B. Mandelbrot, a Polish mathematician, made the Julia sets popular again. Today his work has become one of the most fascinating areas in mathematics.

As with many fractals, Julia sets are derived from a simple process, that very

often leads to highly intricate sets. Consider functions $f : \mathbf{C} \to \mathbf{C}$, where f is a polynomial of degree $n \geq 2$ with complex coefficients:

$$f(z) = a_0 + a_1 z + a_2 z^2 + ... + a_n z^n.$$

Let f^k be the k-fold composition $f \circ f \circ ... \circ f$.

Definition 1

- *The* **escape set** *is defined to be the set of all points z, for which $f^k(z)$ is unbounded ($\to \infty$) as k approaches infinity.*
- *The* **prisoner set** *contains all points z that are not in the escape set.*
- *The* **Julia set** *J is the boundary between the sets of points which iterate to 0 and those which iterate to ∞, i.e. the boundary between the escape and the prisoner set.*

The Julia set is non-empty, compact and usually of fractal structure.

The most often used family of functions, when dealing with Julia sets, are the quadratic ones:

$$f_c(z) = z^2 + c,$$

which are usually used in the following iterative form:

$$z_{n+1} = {z_n}^2 + c, \quad n = 0, 1, 2, \ldots$$

In order to determine in an experiment whether a specific z_n approaches infinity, we need a boundary value r that allows us to conclude: $|z_n| > r$ implies that z is an element of the escape set.

Definition 2 *The value* $r(c) = \max\{|c|, 2\}$ *is called the* **threshold radius.**

Lemma 3.1 *If* z_k *exceeds* $r(c)$ *in absolute value, then the iteration process for* $z \to z^2 + c$ *escapes to infinity.*

Proof: Let c be a fixed parameter, so $r(c) = \max\{|c|, 2\}$. Now assume $|z| \geq |c|$ and $|z| > 2$. There exists a small positive number $\varepsilon > 0$ such that $|z| = 2 + \varepsilon$. Using the triangle inequality for complex numbers, we get:

$$|z^2| = |z^2 + c - c| \leq |z^2 + c| + |c|.$$

This equation implies now:

$$\begin{aligned} |z^2 + c| &\geq |z^2| - |c| \\ &= |z|^2 - |c| \\ &\geq |z|^2 - |z| \\ &= (|z| - 1)|z| \\ &= (1 + \varepsilon)|z|, \end{aligned}$$

so $|z_{n+1}| = |z_n^2 + c| \geq (1 + \varepsilon)|z_n|$. Therefore, after one iteration the absolute value will increase at least by $(1 + \varepsilon)$, after k iterations, it will have increased by at least $(1 + \varepsilon)^k$. Hence the absolute values tend to infinity. ■

In figure 7, we show the Julia set for a quadratic function.

Definition 3 *The* **Mandelbrot set M** *is the set of parameters c for which the Julia set of* f_c *is connected:*

$$M = \{c \in \mathbf{C} : J(f_c) \text{ is connected}\}$$

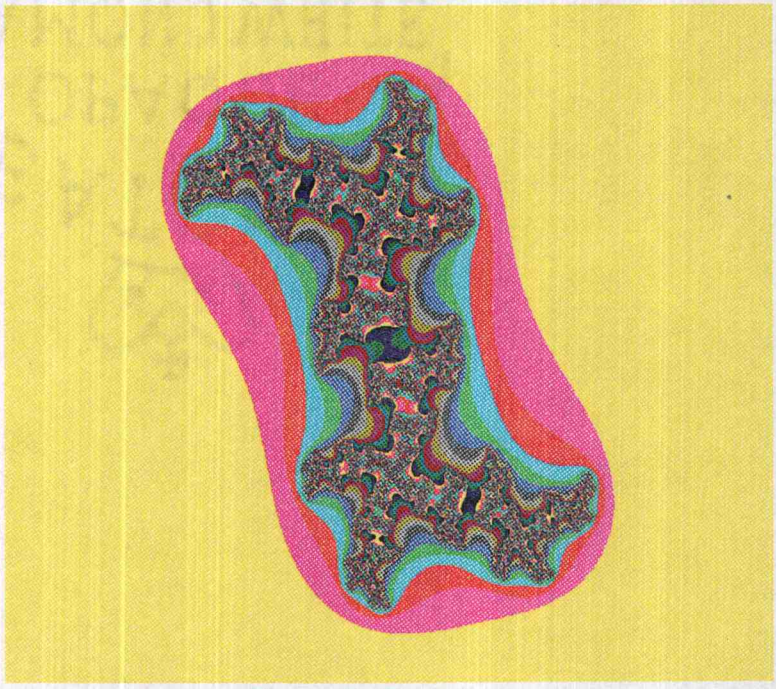

Figure 7. The Julia set

A fact that makes it easier to determine whether a point c belongs to the Mandelbrot set is the following:

Fact: The prisoner set P_c is connected if and only if the critical orbit $0 \to c \to c^2 + c \to \ldots$ is bounded.

A more detailed discussion about this fact can be found in [Peit, 1992]. The above fact allows us to give an alternative definition of the Mandelbrot set.

Definition 4 (alternative) *The* **Mandelbrot set** M *is the set of* c *for which* $0 \to c \to c^2 + c \to \ldots$ *remains bounded:*

$$M = \{c \in \mathbf{C} : 0 \to c \to c^2 + c \to \ \ldots \ \textit{remains bounded}\ \}$$

The Mandelbrot set itself is connected. In figure 8, we show one of the most popular representations of the Mandelbrot set.

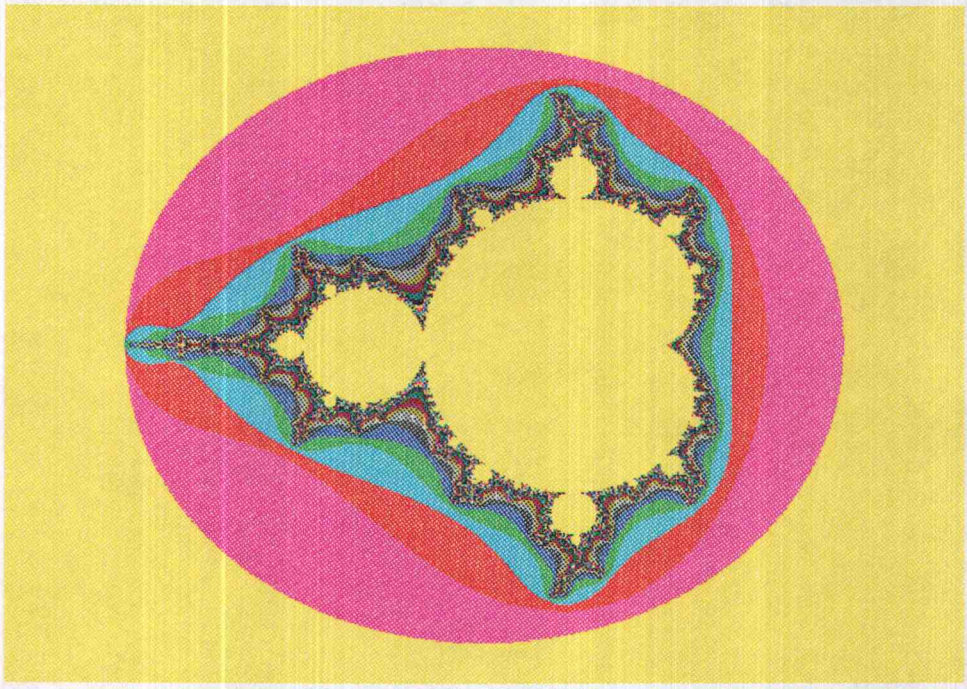

Figure 8. The Mandelbrot set

3.1.4 Strange Attractors

In the discussion of chaos in dynamical systems of two or more dimensions, we find that the notion of *strange attractors* is of importance. Strange attractors occur in dissipative dynamical systems, i.e. systems with some sort of friction. Until recently, scientists believed that the long term behavior of dissipative systems would always run into simple patterns of motion such as a rest point or a limit cycle. But scientists discovered that the long term behavior sometimes moves randomly, but always remains close to a certain set - the attractor. If this set has a fractal structure, we call it *fractal attractor* or *strange attractor*.

We will now introduce several attractors. The first example is the *Hénon attractor*, for which we use a 'stretching and folding' transformation - the Hénon map

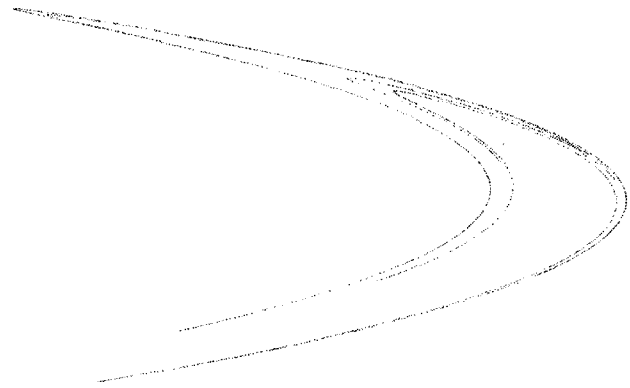

Figure 9. The Hénon attractor for $a = 1.4$ and $b = 0.3$.

$f : \mathbf{R}^2 \rightarrow \mathbf{R}^2$:

$$f(x, y) = (y + 1 - ax^2, bx),$$

where a and b are constants. Hénon used the values $a = 1.4$ and $b = 0.3$, [Heno, 1976]. For these values, we show the Hénon attractor in figure 9. Numerical estimates give a box dimension of about 1.26, see section 3.2.2 and [Falc, 1990].

The second example is the *Lorenz attractor*. Lorenz tried to describe thermal convection. His model does not only describe the motion of some viscous fluid, but also contains information about the distribution of heat. When fluid is heated from below, it rises. Once it reaches the surface, it cools and sinks. This result can be modeled with parallel rotating cylindrical rolls. Lorenz used the continuity equation, the Navier-Stokes equation from fluid dynamics and the heat conduction equation to come up with a description of one of these rolls. After approximating

and simplifying, he stated what are now known as the *Lorenz equations*:

$$\begin{aligned} \frac{dx}{dt} &= \sigma(y - x) \\ \frac{dy}{dt} &= rx - y - xz \\ \frac{dz}{dt} &= xy - bz, \end{aligned}$$

where the variables and constants represent the following:

x: the rate of rotation of the cylinder,

y: the difference in temperature at opposite sides of the cylinder,

z: the deviation from a linear vertical temperature gradient,

σ: the Prandtl number,

r: a control parameter representing the fixed temperature difference between the bottom and the top of the system,

b: a constant depending on the width-to-height ratio of the layer.

Figure 10 shows a Lorenz attractor.

3.2 Dimensions

One of the most important tools, so far, to determine whether or not a set has a fractal structure, is its *dimension.* There are many different definitions of dimension which will give varying results, but they all contain information about the geometric properties of a set and they provide us with a description of how much space is filled by a set. Not all of these definitions are generally applicable.

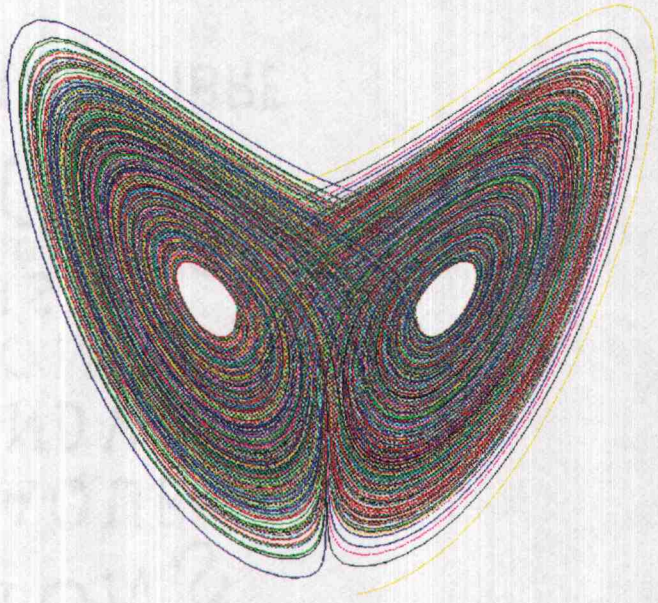

Figure 10. The Lorenz attractor.

3.2.1 Hausdorff Dimension

The notion of *Hausdorff dimension* is the most important concept in defining dimensions in a fractal setting. Mandelbrot defined a fractal as a set whose Hausdorff dimension is strictly greater than its topological dimension. The topological dimension of a set is always an integer and is 0 if it is totally disconnected, 1 if each point has arbitrarily small neighborhoods with boundary of dimension 0, and so on. The Hausdorff dimension has the advantage of being defined for any set and is mathematically convenient since it provides us with a measure-theoretic approach to the problem of finding the dimension of curves and surfaces. Let us have a closer look at this dimension.

Definition 5 *In a metric space (X, ρ), the* **distance** *ρ from a point to a set and the distance between two sets are defined as follows: Let $x \in X$ and let $E, F \subset X$, then:*

$$\rho(x, E) = \inf \{\rho(x, y) : y \in E\},$$

$$\rho(E, F) = \inf \{\rho(x, y) : x \in E, y \in F\}.$$

Definition 6 *The* **diameter** *of U, $U \subset \mathbf{R}^n$ $(U \neq \emptyset)$ is defined to be:*

$$diam\ U = \sup \{\rho(x, y) : x, y \in U\}.$$

Definition 7 *Let $\{U_i\}$ be a countable (or finite) collection of sets of diameter at most δ that cover F, i.e. $F \subset \bigcup_{i=1}^{\infty} U_i$ with $0 < diam\ U_i \leq \delta$, for all i. Then $\{U_i\}$ is a* **δ-cover** *of F.*

Suppose $(\mathbf{R}^n, \rho)$ is a metric space, $s \geq 0$ and $\delta > 0$. Since we are interested in measures of Borel sets, we let F be a Borel set. If $F \subset \mathbf{R}^n$, let

$$\mathcal{H}^s_\delta(F) = \inf\left\{\sum_{i=1}^{\infty}(\text{diam } U_i)^s : \{U_i\} \text{ is a } \delta\text{-cover of } F\right\} \tag{3.1}$$

with the convention that the infimum of an empty set of real numbers is infinite. Thus, we look at all covers of F by sets of diameters at most δ and seek to minimize the sum of the s^{th} powers of the diameters. As δ decreases, the infimum is taken over a smaller family of coverings of F, so that $\mathcal{H}^s_\delta(F)$ increases, and so approaches a limit as $\delta \to 0$. The quantity

$$\mathcal{H}^s(F) = \lim_{\delta \to 0} \mathcal{H}^s_\delta(F) \tag{3.2}$$

is called the **s-dimensional Hausdorff measure** of F. Hausdorff measures generalize the familiar notions of length, area and volume.

For subsets of $\mathbf{R}^n$, n-dimensional Hausdorff measure is, up to a constant multiple, just n-dimensional Lebesgue measure, see e.g. [Foll, 1984].

If F is a Borel subset of $\mathbf{R}^n$, then $\mathcal{H}^n(F) = c_n m_n(F)$, where $m_n(F)$ is the Lebesgue measure of F and $c_n = \pi^{\frac{n}{2}}/\Gamma(\frac{n}{2}+1)$ is the volume of an n-dimensional ball of radius 1. For specific n's we get the following:

If F is a finite number of points:

$\underline{n=0}$: $\mathcal{H}^0(F) = c_0\ vol^0(F) = vol^0(F) =$ number of points of F.

If F is a smooth curve:

$\underline{n=1}$: $\mathcal{H}^1(F) = c_1\ vol^1(F) = 2\ vol^1(F) =$ length of F.

If F is a smooth surface:

$\underline{n=2}: \mathcal{H}^2(F) = c_2\ vol^2(F) = \pi\ area(F).$

If F is a 3-dimensional volume:

$\underline{n=3}: \mathcal{H}^3(F) = c_3\ vol^3(F) = \frac{4\pi}{3}\ volume(F).$

Equation (3.1) implies that $\mathcal{H}^s_\delta(F)$ is non-increasing in s for all F and for all δ less than 1. This statement together with equation (3.2) implies that $\mathcal{H}^s(F)$ is also non-increasing. If $t > s$ and $\{U_i\}$ is a δ-cover of F, we have:

$$\begin{aligned}
\text{diam } U_i &\leq \delta \\
(\text{diam } U_i)^{t-s} &\leq \delta^{t-s} \\
(\text{diam } U_i)^t &\leq (\text{diam } U_i)^s \delta^{t-s} \\
\sum_{i=1}^{\infty}(\text{diam } U_i)^t &\leq \delta^{t-s} \sum_{i=1}^{\infty}(\text{diam } U_i)^s \\
\inf \sum_{i=1}^{\infty}(\text{diam } U_i)^t &\leq \delta^{t-s} \inf \sum_{i=1}^{\infty}(\text{diam } U_i)^s \\
\mathcal{H}^t_\delta(F) &\leq \delta^{t-s}\mathcal{H}^s_\delta(F).
\end{aligned}$$

Let $\delta \to 0$. If $\mathcal{H}^s(F) < \infty$, then $\mathcal{H}^t(F) = 0$ for $t > s$. Thus a graph of $\mathcal{H}^s(F)$ versus s shows that there is a critical value of s at which $\mathcal{H}^s(F)$ jumps from ∞ to 0, as one can see in figure 11. This value is called **Hausdorff dimension** of F, denoted by:

$$\dim_H(F) = \inf\{s : \mathcal{H}^s(F) = 0\} = \sup\{s : \mathcal{H}^s(F) = \infty\},$$

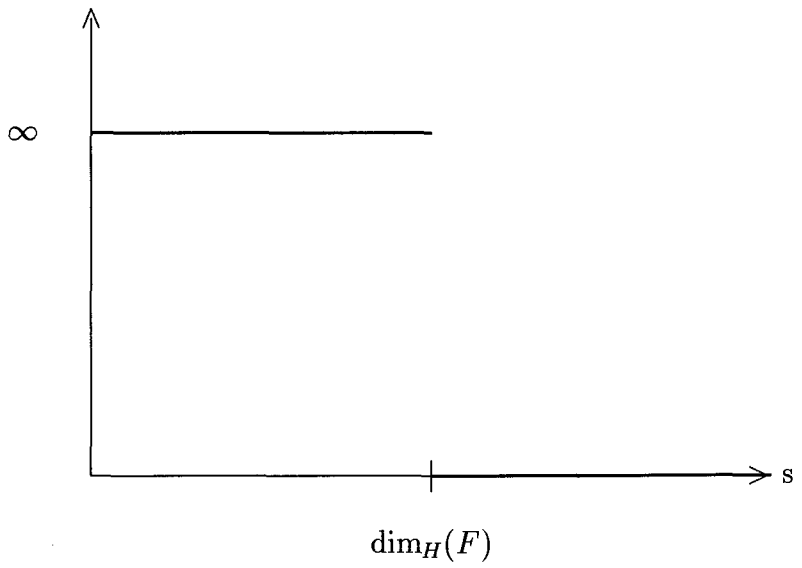

Figure 11. An illustration of the Hausdorff dimension.

so that

$$\mathcal{H}^s(F) = \begin{cases} \infty & \text{if } s < \dim_H(F) \\ 0 & \text{if } s > \dim_H(F) \\ c & \text{if } s = \dim_H(F), \text{ where } 0 \leq c \leq \infty. \end{cases}$$

Simple example: Let F be a ball with radius 1 in $\mathbf{R}^4$. Then:

$$\begin{aligned} \mathcal{H}^1(F) &= 2 \text{ length}(F) = \infty, \\ \mathcal{H}^2(F) &= \pi \text{ area}(F) = \infty, \\ \mathcal{H}^3(F) &= \frac{4\pi}{3} \text{ volume}(F) < \infty, \\ \mathcal{H}^4(F) &= c_4 \, vol^4(F) = 0. \end{aligned}$$

Therefore, $\dim_H(F) = 3$ with $\mathcal{H}^s(F) = \infty$ if $s < 3$ and $\mathcal{H}^s(F) = 0$ if $s > 3$.

In the next example, we will show how one finds the dimension of the Cantor set using the Hausdorff dimension.

Example: Let F be the middle third Cantor set, introduced in section 3.1.1. If $s = \frac{\log 2}{\log 3} = .6309$, then $\dim_H(F) = s$ and $1/2 \leq \mathcal{H}^s(F) \leq 1$.

Proof: Recall that after the k^{th} construction step, the set E_k is a collection of 2^k intervals of length 3^{-k}. If we let k go to infinity, we obtain the Cantor set F, i.e. $F = \lim_{k\to\infty} E_k$.

Let $\{U_i\}$ be the covering of F consisting of the 2^k intervals of length 3^{-k}. Since $\delta = 3^{-k}$ and $(\text{diam } U_i) = |U_i|$, we can write:

$$\begin{aligned} \mathcal{H}^s_\delta(F) &= \inf\{\sum_{i=1}^{\infty}(\text{diam } U_i)^s : \{U_i\} \text{ is a } \delta\text{-cover of } F\} \\ \mathcal{H}^s_{3^{-k}}(F) &\leq \sum_{i=1}^{\infty}(|U_i|)^s \\ \mathcal{H}^s_{3^{-k}}(F) &\leq 2^k 3^{-ks}. \end{aligned}$$

Using the assumption $s = \frac{\log 2}{\log 3}$, we find:

$$\mathcal{H}^s_{3^{-k}}(F) \leq 1.$$

Letting δ go to zero, we obtain:

$$\mathcal{H}^s(F) = \lim_{\delta\to 0} \mathcal{H}^s_\delta(F) = \lim_{k\to\infty} \mathcal{H}^s_{3^{-k}}(F) \leq 1.$$

Now, to prove that $\mathcal{H}^s(F) \geq 1/2$, it suffices to show that

$$\sum_i (|U_i|)^s \geq 1/2 = 3^{-s} \tag{3.3}$$

for any cover cover $\{U_i\}$ of F.

We assume, without loss of generality, that the $\{U_i\}$ are intervals, and by expanding them slightly, we need only verify (3.3) if $\{U_i\}$ is a finite collection of closed

subintervals in $[0,1]$.

For each U_i, we will choose k to be the integer such that

$$3^{-(k+1)} \leq |U_i| < 3^{-k}. \tag{3.4}$$

Therefore, U_i can intersect at most one of the intervals that determine E_k (since they are separated by a distance of at least 3^{-k}). If $j \geq k$, then by construction, U_i intersects at most $2^{j-k} = 2^j 3^{-sk} \leq 2^j 3^s |U_i|^s$ of the intervals, using (3.4). If we choose j large enough, so that $3^{-(j+1)} \leq |U_i|$, for all U_i, then $\{U_i\}$ intersects all 2^j intervals of length 3^{-j}. Counting the intervals gives $2^j \leq \sum_i 2^j 3^s |U_i|^s$, which reduces to (3.3). We have shown that $1/2 \leq \mathcal{H}^s(F) \leq 1$, if $s = \frac{\log 2}{\log 3}$. This implies that for $s < \frac{\log 2}{\log 3}$, $\mathcal{H}^s(F) = \infty$ and for $s > \frac{\log 2}{\log 3}$, $\mathcal{H}^s(F) = 0$. Thus $\dim_H(F) = \frac{\log 2}{\log 3}$, which is non-integer and therefore fractal. ■

3.2.2 Box Counting Dimension

The box-counting dimension is one of the most widely used dimensions, since it is easily applicable. Other names for the box-counting dimension are 'Kolmogorov entropy', 'entropy dimension', 'capacity dimension', 'metric dimension', 'logarithmic density' and 'information dimension'.

Definition 8 *Let F be any nonempty bounded subset of $\mathbf{R}^n$, then the* **lower** *and* **upper box-counting dimension** *of F, respectively, are defined as:*

$$\underline{\dim}_B(F) = \liminf_{\delta \longrightarrow 0} \frac{\log N_\delta(F)}{-\log \delta},$$

$$\overline{\dim}_B(F) = \limsup_{\delta \longrightarrow 0} \frac{\log N_\delta(F)}{-\log \delta}.$$

If these are equal, then the common value is called the **box-counting dimension** *of F:*

$$\dim_B(F) = \lim_{\delta \to 0} \frac{\log N_\delta(F)}{-\log \delta},$$

where $N_\delta(F)$ is any of the following:

- *the smallest number of closed balls of radius δ that cover F;*
- *the smallest number of cubes of side δ that cover F;*
- *the number of δ-mesh cubes that intersect F;*
- *the smallest number of sets of diameter at most δ that cover F;*
- *the largest number of disjoint balls of radius δ with centers in F.*

In practice one adopts the definition most convenient for a particular application. An equivalent definition of box-counting dimension of a rather different form can be introduced, starting out from the following.

Definition 9 *The* **δ-parallel body** *F_δ of F is*

$$F_\delta = \{x \in \mathbf{R}^n : |x - y| \leq \delta \text{ for some } y \in F\},$$

i.e. the set of points within distance δ of F.

We consider now the rate at which the n-dimensional volume of F_δ shrinks as $\delta \to 0$. If F is a single point in $\mathbf{R}^3$, then the 'ball-like' volume of F_δ equals $vol(F_\delta) = \frac{4}{3}\pi\delta^3$.

If F is a segment of length l in $\mathbf{R}^3$, then the 'sausage-like' volume of F_δ equals $vol(F_\delta) \approx \pi l \delta^2$. If F is a flat set of area a in $\mathbf{R}^3$, then the volume of F_δ equals $vol(F_\delta) \approx 2a\delta$. In each case, we get $vol(F_\delta) \approx c\delta^{3-s}$, where s is the dimension of F and c a constant.

Definition 10 *Let F be a subset of $\mathbf{R}^n$. If for some s, $\delta^{s-n} vol^n(F_\delta)$ tends to a positive finite limit as $\delta \to 0$, we define F as s-dimensional and the limiting value as the* **s-dimensional content** *of F.*

The s-dimensional content has a restricted usage. Since it is not a measure, it is not necessarily additive on disjoint sets.

3.2.3 Similarity Dimension

The property of self-similarity or scaling, as exemplified by the von-Koch curve, the Cantor set, the Mandelbrot set, etc. is one of the central concepts of fractional geometry. An object normally considered as one-dimensional can be divided into N identical parts, each of which is scaled down by the ratio $r = \frac{1}{N}$. Similarly, a two dimensional object such as a square area in a plane can be divided into N self-similar parts, each of which is scaled down by a factor $r = \frac{1}{\sqrt{N}}$. So, in general, a D-dimensional self-similar object can be divided into N smaller copies of itself, each of which is scaled down by a factor r, where

$$r = \frac{1}{N^{\frac{1}{D}}}, \quad N = \frac{1}{r^D}, \quad Nr^D = 1.$$

This now defines the **fractal (similarity) dimension** D:

$$D = \frac{\log N}{\log \frac{1}{r}}$$

The fractal dimension need not be an integer, which will be the most interesting case when one talks about fractals. Fractals will not have an integer dimension.

Examples:

1. Von-Koch Curve: Any segment of the von-Koch curve is composed of 4 sub-segments, each of which is scaled down by a factor $\frac{1}{3}$ from the beginning segment. Its fractal dimension is $D = \frac{\log 4}{\log 3} \approx 1.26$. This non-integral dimension reflects the unusual properties of the curve.

2. Cantor Set: Any segment of the Cantor set is composed of 2 sub-segments, each of which is scaled down by a factor $\frac{1}{3}$ from the first segment. Its fractal dimension is $D = \frac{\log 2}{\log 3} \approx .63$.

The concept of fractal dimension can also be applied to statistically self-similar objects, such as a coastline.

Chapter 4

Analysis of the Wave Equation

It was shown in the preceding chapter that the behavior of certain surface waves is governed by the following equation:

$$h_t + \mu h h_x = \sigma \frac{h_{xx}}{(1+h_x^2)^{3/2}} - \varrho h g. \tag{4.1}$$

In order to study the solutions to this partial differential equation under various conditions, it is convenient to nondimensionalize it. Let

$$h = Hu, \quad x = L\xi, \quad t = T\tau. \tag{4.2}$$

Here u, ξ, τ are dimensionless variables thought of as 'order one' and H, L, T are constants which give the typical dimension for the problem. Applying the transformation (4.2) to (4.1), we get:

$$\begin{aligned} HT^{-1}u_\tau + \mu H^2 L^{-1} u u_\xi &= \sigma H L^{-2} u_{\xi\xi}(1 + H^2 L^{-2} u_\xi^2)^{-3/2} - \varrho g H u \\ u_\tau + \mu H T L^{-1} u u_\xi &= \sigma T L^{-2} u_{\xi\xi}(1 + H^2 L^{-2} u_\xi^2)^{-3/2} - \varrho g T u. \end{aligned}$$

Since H, L and T are typical constants, which means they are suitable to the problem, we can choose them such that $\mu HTL^{-1} = 1$. Then:

$$u_\tau + uu_\xi = \sigma(\mu HL)^{-1}u_{\xi\xi}(1 + H^2L^{-2}u_\xi^2)^{-3/2} - \varrho gL(\mu H)^{-1}u. \tag{4.3}$$

Let $\varepsilon = HL^{-1}$, $\delta = \sigma(\mu HL)^{-1} = \sigma(\mu\varepsilon L^2)^{-1}$ and $\eta = \varrho gL(\mu H)^{-1} = \varrho g(\mu\varepsilon)^{-1}$. Applying these substitutions to (4.3), we obtain the wave equation represented in the following form:

$$u_\tau + uu_\xi = \delta u_{\xi\xi}(1 + \varepsilon^2 u_\xi^2)^{-3/2} - \eta u. \tag{4.4}$$

In order to solve this equation, it will be convenient to split it up into several cases, representing certain conditions. Any of the parameters δ, ε and η, which constitute physical properties, might be assumed to be small so that corresponding terms in (4.4) can be ignored. This leads to six different cases, which we shall analyze separately:

- Case a: δ, η small, ε arbitrary $\Rightarrow u_\tau + uu_\xi = 0$.
- Case b: δ small, ε, η arbitrary $\Rightarrow u_\tau + uu_\xi = -\eta u$.
- Case c: ε, η small, δ arbitrary $\Rightarrow u_\tau + uu_\xi = \delta u_{\xi\xi}$.
- Case d: ε small, δ, η arbitrary $\Rightarrow u_\tau + uu_\xi = \delta u_{\xi\xi} - \eta u$.
- Case e: η small, ε, δ arbitrary $\Rightarrow u_\tau + uu_\xi = \delta u_{\xi\xi}(1 + \varepsilon^2 u_\xi^2)^{-3/2}$.
- Case f: $\delta, \eta, \varepsilon$ arbitrary $\Rightarrow u_\tau + uu_\xi = \delta u_{\xi\xi}(1 + \varepsilon^2 u_\xi^2)^{-3/2} - \eta u$.

Several cases look familiar (e.g. Burgers' equation in case c) and we know that the solution represents a smooth surface. Several authors, however, claim that the solution to the wave equation is a "rough" (fractal) surface (e.g. [Stia, 1991], [Hass, 1962], [Zakh, 1982]). Stiassnie [Stia, 1991] models the free-surface elevation, neglecting the surface tension. He combines the linear model of Pierson and the stochastic model of Hasselmann [Hass, 1962]. As a result, he finds an indication of the possibility that the free surface of the ocean can become a fractal with dimension of about 2.3. In the one-dimensional case, the dimension would be about 1.3. In [Hass, 1962], Hasselmann uses a stochastic model to describe waves. The energy flux in a gravity wave results from weak, non-linear couplings between the spectral components. As the interactions are weak, it can be deduced from a loose application of the Central Limit Theorem, that in the linear approximation a wind-generated random sea is Gaussian. Hasselmann evaluates the energy flux, using a perturbation method. In [Pier, 1955], it is also shown that we can model the free-surface elevation by a multivariate Gaussian process. We shall show later that the solution to cases (e) and (f) is indeed a non-smooth surface.

Before we continue solving each case, we shall find it convenient to state the following four lemmas:

Lemma 4.1

$$e^{-ax^2} = \frac{1}{\sqrt{4a\pi}} \int_{-\infty}^{\infty} e^{-i\omega x - \omega^2 (4a)^{-1}} d\omega$$

Proof: An excellent discussion about this proof can be found in [Guen, 1988].

Lemma 4.2

$$\int_0^t |\ln\tau|\tau^n d\tau \leq \frac{t^{n+1}}{n+1}\left\{\frac{1}{n+1} + |\ln t|\right\}$$

Proof:

$$\int_0^t |\ln\tau|\tau^n d\tau = \begin{cases} \int_0^t (-\tau^n \ln\tau) d\tau & \text{if } t < 1 \\ \int_0^1 (-\tau^n \ln\tau) d\tau + \int_1^t (\tau^n \ln\tau) d\tau & \text{if } t \geq 1 \end{cases}$$

Using partial integration, we find:

$$\begin{aligned} \int_0^t |\ln\tau|\tau^n d\tau &= \begin{cases} -\frac{1}{n+1}\, t^{n+1}\ln t + \int_0^t \frac{1}{n+1}\tau^n d\tau & \text{if } t < 1 \\ \int_0^1 \frac{1}{n+1}\tau^n d\tau + \frac{1}{n+1}\, t^{n+1}\ln t - \int_1^t \frac{1}{n+1}\tau^n d\tau & \text{if } t \geq 1 \end{cases} \\ &= \begin{cases} \frac{1}{n+1}\, t^{n+1}\left\{\frac{1}{n+1} - \ln t\right\} & \text{if } t < 1 \\ \frac{1}{n+1}\left\{\frac{2}{n+1} + t^{n+1}\left\{\ln t - \frac{1}{n+1}\right\}\right\} & \text{if } t \geq 1. \end{cases} \end{aligned}$$

If we consider the fact that $2 \leq 2t$ for all $t \geq 1$, we find:

$$\begin{aligned} \int_0^t |\ln\tau|\tau^n d\tau &\leq \begin{cases} \frac{1}{n+1}\, t^{n+1}\left\{\frac{1}{n+1} - \ln t\right\} & \text{if } t < 1 \\ \frac{1}{n+1}\, t^{n+1}\left\{\frac{1}{n+1} + \ln t\right\} & \text{if } t \geq 1 \end{cases} \\ &= \frac{1}{n+1}\, t^{n+1}\left\{\frac{1}{n+1} + |\ln t|\right\}. \end{aligned}$$

■

Lemma 4.3 *Let* $\varphi(x,t) = \exp(-\frac{1}{2\delta}\int_0^x u(y,t)dy + \mu(t))$, *where* $\delta > 0$. *If* $u \in L_1$, *then* $0 < m \leq |\varphi| \leq M$ *and*

$$|\ln \varphi| \leq \ln D \quad or \quad |\ln \varphi| \leq |\ln Dt|,$$

where D *is a constant and* t *is fixed.*

Proof: To find the upper bound on $|\varphi|$, we will consider the absolute value

$$|\varphi(x,t)| = |e^{\mu(t)}||e^{-1/(2\delta)\int_0^x u(y,t)dy}|.$$

Since t is fixed, $N = |e^{\mu(t)}|$, therefore:

$$|\varphi(x,t)| \leq Ne^{|-1/(2\delta)\int_0^x u(y,t)dy|}.$$

The exponential function is strictly increasing, therefore we obtain:

$$\begin{aligned} |\varphi(x,t)| &\leq Ne^{1/(2\delta)\int_0^x |u(y,t)|dy} \\ &\leq Ne^{1/(2\delta)\int_{-\infty}^{\infty} |u(y,t)|dy}. \end{aligned}$$

Since u is a function of L_1, the integral in the exponent is bounded:

$$|\varphi(x,t)| \leq M.$$

There exists a positive lower bound for φ, since the exponential function is strictly increasing:

$$\begin{aligned} |\varphi(x,t)| &= Ne^{-1/(2\delta)\int_0^x u(y,t)dy} \\ &\geq Ne^{-1/(2\delta)\int_0^x |u(y,t)|dy}. \end{aligned}$$

The integral in the exponent being bounded implies that the right hand side of the equation above is strictly larger than zero. Therefore, for fixed $t > 0$:

$$0 < m \leq \varphi \leq M < \infty \quad \text{or} \quad 0 < mt \leq \varphi \leq Mt < \infty.$$

Let $\ln D = \max\{|\ln m|, |\ln M|\}$ or $|\ln Dt| = \max\{|\ln mt|, |\ln Mt|\}$, then:

$$|\ln \varphi| \leq \ln D \text{ or } |\ln \varphi| \leq |\ln Dt|.$$

■

Another helpful fact is that the fundamental solution of the heat equation is normalized:

Lemma 4.4

$$\int_{-\infty}^{\infty} k(x,t)dx = 1,$$

where $k(x,t) = \frac{1}{\sqrt{4\pi t}} \exp\left(-\frac{x^2}{4t}\right)$ *is the fundamental solution of the heat equation.*

Proof: A proof of this lemma can be found in most probability books.

4.1 Case a: $u_t + uu_x = 0$

This partial differential equation, which is the case where $\delta = 0$ in **Burgers' equation**, can be solved using the *method of characteristics*:

$$\frac{dx}{dt} = u, \quad \text{i.e. } x'(t) = u(x(t), t).$$

Since we know that u is constant along characteristics, we can conclude that $x'(t)$ is also constant along the characteristic lines. Therefore the characteristics have to be straight lines. Given the profile of the initial condition $u_0(x) = u(x, 0)$, we shall be able to determine the shape of the characteristics. If $u_0'(x)$ is not larger than or equal to 0 for all x, then shockwaves will appear. The shock velocity will be $\frac{1}{2}(u_l + u_r)$, where u_l and u_r are the values of u on the left and right hand side of the shock, respectively. Since we consider waves, the case where $u_0'(x)$ is larger than or equal to 0 for all x will never appear. Therefore shockwaves will always occur.

Example: Let us consider the above case of Burgers' equation, with the initial condition $u(x, 0) = \sin(x)$:

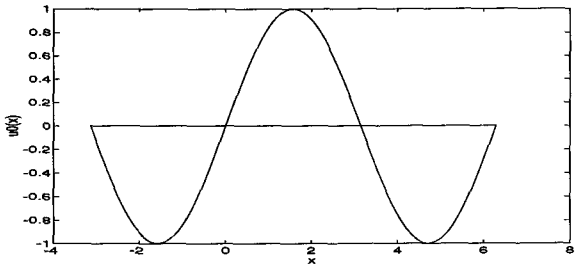

Figure 12. Initial condition for $u_t + uu_x = 0$

Since the first derivative of this initial condition is not larger than or equal to 0 for all x, we get crossing characteristic lines, as one can see in figure 13. The crossing characteristics indicate that a shock wave should appear. Figure 14 shows the solution of $u_t + uu_x = 0$. As expected, an almost vertical line appears, indicating where the shockwave would be.

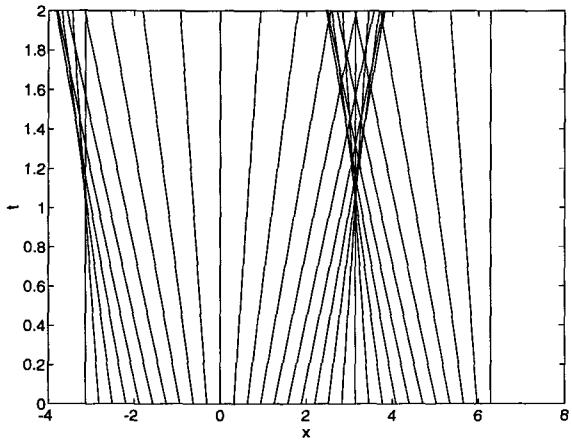

Figure 13. Characteristics of $u_t + uu_x = 0$

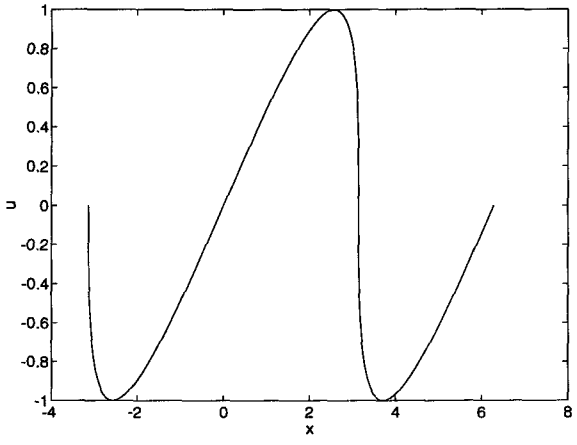

Figure 14. Shock wave at $t = 1$

4.2 Case b: $u_t + uu_x = -\eta u$

This partial differential equation is the damped **Burgers' equation** with $\delta = 0$. Analogously to case a, we will solve it using the method of characteristics. Let

$$\frac{dt}{d\tau} = 1, \qquad \frac{dx}{d\tau} = u, \qquad \frac{du}{d\tau} = -\eta u. \tag{4.5}$$

We solve the three ordinary differential equations in (4.5), and determine the constants using the initial condition $u(x,0) = f(x)$, which we parametrize as $x_0(s) = s$, $t_0(s) = 0$ and $u_0(s) = f(s)$.

1. $t = \tau + c$

   Using the initial condition ($\tau = 0$), we find $c = 0$. Therefore:

   $$t = \tau. \tag{4.6}$$

2. $\frac{du}{d\tau} = -\eta u$

   By separating variables, we find:

   $$\begin{aligned} \frac{du}{u} &= -\eta d\tau \\ u &= Ce^{-\eta\tau}. \end{aligned}$$

   Using the initial condition, we determine $u_0(s) = C = f(s)$. Therefore:

   $$u = f(s)e^{-\eta\tau}. \tag{4.7}$$

3. $\frac{dx}{d\tau} = u$

   If we substitute the result we found in (4.7) for u, we get:

   $$\frac{dx}{d\tau} = f(s)e^{-\eta\tau}.$$

Applying the method of separating variables and integrating, we find:

$$x = -\frac{1}{\eta} f(s) e^{-\eta\tau} + K$$

To find the constant K, we use the initial condition:

$$\begin{aligned} x_0(s) &= -\frac{1}{\eta} f(s) + K(s) = s \\ \Rightarrow K(s) &= s + \frac{1}{\eta} f(s) \end{aligned}$$

Therefore,

$$x = -\frac{1}{\eta} f(s) e^{-\eta\tau} + \frac{1}{\eta} f(s) + s. \tag{4.8}$$

The solution of $u_t + uu_x = -\eta u$ is now represented by the following system of equations, which contains (4.6), (4.7) and (4.8):

$$\begin{aligned} t &= \tau \\ u &= f(s) e^{-\eta\tau} \\ x &= \frac{1}{\eta} f(s) \left(1 - e^{-\eta\tau}\right) + s. \end{aligned}$$

We can transform these three equations into:

$$\begin{aligned} u &= f(s) e^{-\eta t} \\ x &= \frac{1}{\eta} f(s) \{1 - e^{-\eta t}\} + s \end{aligned}$$

and graph them using the initial condition $f(x) = \sin x$, as shown in figures 15 and 16.

Starting with the sine curve at $t = 0$, the solution flattens out as t gets larger.

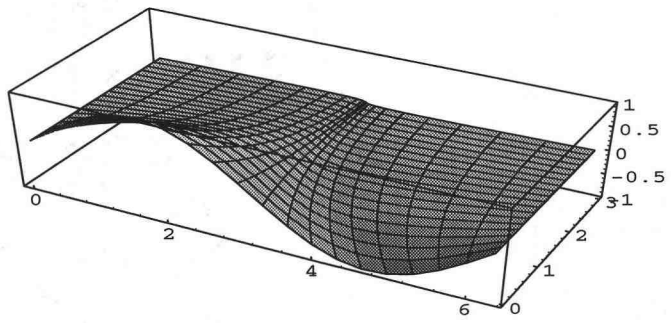

Figure 15. Wave for t = 0 to t = 3

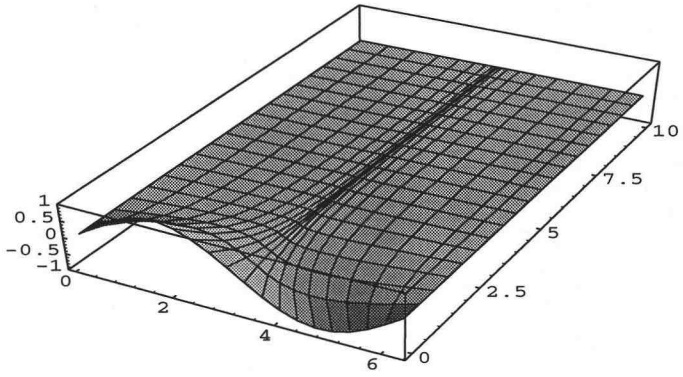

Figure 16. Wave for t = 0 to t = 10

4.3 Case c: $u_t + uu_x = \delta u_{xx}$

In this section, we will consider the standard **Burgers' equation**:

$$u_t + uu_x = \delta u_{xx}.$$

This can be written in form of a conservation law, where we have a time derivative on one side of the equality, and a space derivative on the other side.

$$u_t = (\delta u_x - \frac{1}{2}u^2)_x. \tag{4.9}$$

In order to solve this conservation law, we use the following substitution, suggested in [Hopf, 1950]:

$$u = -2\delta\frac{\varphi_x}{\varphi} = -2\delta(\ln|\varphi|)_x, \tag{4.10}$$

where $\delta > 0$.

Substituting (4.10) into (4.9), we get:

$$\begin{aligned} -2\delta(\ln\varphi)_{xt} &= \left(-2\delta^2\left(\frac{\varphi_{xx}}{\varphi} - \frac{{\varphi_x}^2}{\varphi^2}\right) - 2\delta^2\frac{{\varphi_x}^2}{\varphi^2}\right)_x \\ \Leftrightarrow \qquad -(\ln\varphi)_{tx} &= \left(-\delta\frac{\varphi_{xx}}{\varphi}\right)_x. \end{aligned}$$

We will integrate both sides with respect to the x-variable, which leads to:

$$\begin{aligned} -\frac{\varphi_t}{\varphi} &= -\delta\frac{\varphi_{xx}}{\varphi} - c(t) \\ \Leftrightarrow \qquad \varphi_t &= \delta\varphi_{xx} + c(t)\varphi. \end{aligned} \tag{4.11}$$

After these transformations, we obtain a partial differential equation that appears easier to solve than (4.9), especially because it reminds us of the heat equation.

If we let $\varphi = \varphi \exp \int c\,dt$, the last term in the equation (4.11) will vanish. This results in the **heat equation**:

$$\varphi_t = \delta \varphi_{xx}. \tag{4.12}$$

We now have to solve the following restated problem:

$$\begin{aligned} &\varphi_t - \delta\varphi_{xx} = 0, \qquad -\infty < x < \infty, \qquad t > 0, \\ &\varphi(x,0) = f(x), \qquad -\infty < x < \infty. \end{aligned} \tag{4.13}$$

There exist several different ways to solve the heat equation. It turns out that in our case, the most convenient method is the one using Fourier transforms. Recall that a sufficiently well-behaved function has a Fourier transform:

$$\hat{\varphi}(\omega) = \int_{-\infty}^{\infty} e^{i\omega x}\varphi(x)dx.$$

The inverse Fourier transform is given by:

$$\varphi(x) = \frac{1}{2\pi}\int_{-\infty}^{\infty} e^{-i\omega x}\hat{\varphi}(\omega)d\omega. \tag{4.14}$$

To write the heat equation using the Fourier transform of φ, we multiply equation (4.14) by $e^{i\omega x}$, and integrate over x from $-\infty$ to ∞:

$$\int_{-\infty}^{\infty} e^{i\omega x}(\varphi_t - \delta\varphi_{xx})dx = 0.$$

Assuming $\varphi_x, \varphi \to 0$ as $x \to \pm\infty$, we obtain:

$$\begin{aligned} 0 &= \frac{\partial}{\partial t}\int_{-\infty}^{\infty} e^{i\omega x}\varphi dx + \delta\omega^2 \int_{-\infty}^{\infty} e^{i\omega x}\varphi dx \\ &= \hat{\varphi}_t(\omega,t) + \delta\omega^2\hat{\varphi}(\omega,t). \end{aligned}$$

The problem stated in (4.14) is therefore equivalent to:

$$\hat{\varphi}_t = -\delta\omega^2\hat{\varphi}, \qquad \hat{\varphi}(\omega, 0) = \hat{f}(\omega), \tag{4.15}$$

which is an ordinary differential equation, solvable using *separation of variables*:

$$\begin{aligned} \frac{d\hat{\varphi}}{\hat{\varphi}} &= -\delta\omega^2 dt \\ \hat{\varphi} &= Ce^{-\delta\omega^2 t}. \end{aligned}$$

To find the constant C, we use the initial condition given in (4.15):

$$\hat{\varphi} = \hat{f}(\omega)e^{-\delta\omega^2 t}. \tag{4.16}$$

We now found a solution of the heat equation, which contains the Fourier transform of φ. To find a solution for our original φ, we apply the inverse Fourier transform, given in (4.14) to equation (4.16) and obtain the following:

$$\varphi(x,t) = \frac{1}{2\pi}\int_{-\infty}^{\infty} \hat{f}(\omega)e^{-i\omega x - \delta\omega^2 t}\, d\omega.$$

Now we have to apply (4.14) to $\hat{f}(\omega)$, which gives us:

$$\varphi(x,t) = \frac{1}{2\pi}\int_{-\infty}^{\infty} e^{-i\omega x - \delta\omega^2 t}\left(\int_{-\infty}^{\infty} e^{i\omega y} f(y)dy\right) d\omega. \tag{4.17}$$

Changing the order of integration, we find:

$$\varphi(x,t) = \frac{1}{2\pi}\int_{-\infty}^{\infty}\left(\int_{-\infty}^{\infty} e^{-i\omega(x-y)-\delta\omega^2 t} d\omega\right) f(y)\, dy. \tag{4.18}$$

Lemma 4.1 gives the solution of the 'inner' integral and we find that the explicit solution of the heat equation is the following:

$$\varphi(x,t) = \frac{1}{\sqrt{4\delta\pi t}}\int_{-\infty}^{\infty} e^{-\frac{(x-y)^2}{4\delta t}} f(y)\, dy, \tag{4.19}$$

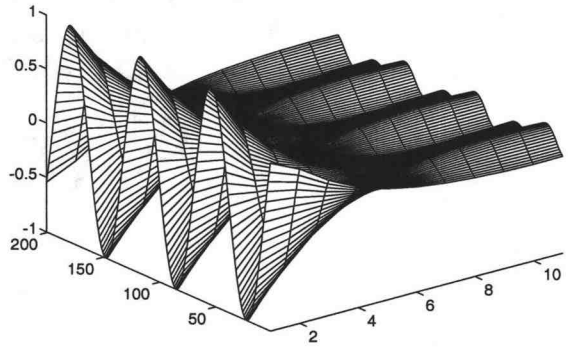

Figure 17. Solution of $u_t + uu_x = \delta u_{xx}$

where $f(y)$ is the initial condition.

As in the examples before, our initial condition is a sine curve. In this case the developing surface smoothes out for large t.

4.4 Case d: $u_t + uu_x = \delta u_{xx} - \eta u$

In this section, we will consider the damped **Burgers' equation**:

$$u_t + uu_x = \delta u_{xx} - \eta u. \tag{4.20}$$

In order to solve equation (4.20), we use the same method as in case c. We will transform parts of equation (4.20) into a conservation law. We then get:

$$\begin{aligned} u_t &= \delta u_{xx} - uu_x - \eta u \\ \Leftrightarrow \quad u_t &= (\delta u_x - \frac{1}{2}u^2)_x - \eta u. \end{aligned} \tag{4.21}$$

Following [Hopf, 1950], we use the substitution

$$u = -2\delta\frac{\varphi_x}{\varphi} = -2\delta(\ln\varphi)_x \tag{4.22}$$

in order to solve (4.21). Substituting (4.22) in equation (4.21), we find:

$$\begin{aligned} -2\delta(\ln\varphi)_{xt} &= \left(-2\delta^2\left(\frac{\varphi_{xx}}{\varphi} - \frac{{\varphi_x}^2}{\varphi^2}\right) - 2\delta^2\frac{{\varphi_x}^2}{\varphi^2}\right)_x + 2\eta\delta(\ln\varphi)_x \\ \Leftrightarrow \qquad -(\ln\varphi)_{tx} &= \left(-\delta\frac{\varphi_{xx}}{\varphi} + \eta\ln\varphi\right)_x. \end{aligned}$$

Integrating this equality with respect to x, we get:

$$\begin{aligned} -\frac{\varphi_t}{\varphi} &= -\delta\frac{\varphi_{xx}}{\varphi} + \eta\ln\varphi + c(t) \\ \Leftrightarrow \qquad -\varphi_t &= -\delta\varphi_{xx} + \eta\ln\varphi\varphi + c(t)\varphi \\ \Leftrightarrow \qquad \varphi_t - \delta\varphi_{xx} &= -\eta\ln\varphi\varphi - c(t)\varphi. \end{aligned} \tag{4.23}$$

Let

$$Q(x,t) = -\eta\ln\varphi\varphi - c(t)\varphi, \tag{4.24}$$

then we obtain:

$$\varphi_t - \delta\varphi_{xx} = Q(x,t). \tag{4.25}$$

We have found an equation that looks very similar to the heat equation. To solve this partial differential equation, we will use the fundamental solution of the heat equation:

$$v(y,\tau) = k(x-y, \delta(t-\tau)), \tag{4.26}$$

where $k(x,t) = \frac{1}{\sqrt{4\pi t}}\exp\left(-\frac{x^2}{4t}\right)$, and the property of v, that $v_t + \delta v_{xx} = 0$, which allows us to write (4.25) as:

$$vQ = v(\varphi_\tau - \delta\varphi_{yy}) + \varphi(v_\tau + \delta v_{yy})$$

$$= (v\varphi)_\tau + \delta(v_{yy}\varphi + v_y\varphi_y - v_y\varphi_y - v\varphi_{yy})_y$$

$$= (v\varphi)_\tau + \delta(\varphi v_y - v\varphi_y)_y. \tag{4.27}$$

Integrating both sides of equation (4.27) from $-R < y < R$ and $0 < \tau < t - \varepsilon$ results in:

$$\begin{aligned}\int_{-R}^{R}\int_0^{t-\varepsilon} v\,Q\,d\tau\,dy &= \int_{-R}^{R} v\varphi|_0^{t-\varepsilon}dy + \delta\int_0^{t-\varepsilon}(\varphi v_y - v\varphi_y)|_{-R}^{R}\,d\tau \\ &= \int_{-R}^{R}(k(x-y,\delta\varepsilon)\varphi(y,t-\varepsilon) - k(x-y,\delta t)\varphi(y,0))dy \\ &\quad +\delta\int_0^{t-\varepsilon}(\varphi v_y - v\varphi_y)|_{-R}^{R}\,d\tau. \end{aligned}\tag{4.28}$$

Assuming φ and φ_x satisfy the growth estimates $|\varphi|, |\varphi_x| \leq 2M\exp(\mu x^2)$ and using the fact that $|v(x,t)|$ and $|v_x(x,t)|$ tend to zero as $x \to \infty$, we find that $(\varphi v_y - v\varphi_y)|_{-R}^{R}$ approaches zero as $R \to \infty$. Therefore,

$$\int_0^{t-\varepsilon}(\varphi v_y - v\varphi_y)|_{-R}^{R}d\tau \to 0 \text{ as } |R| \to \infty$$

and equation (4.28) can be written as:

$$\int_{-R}^{R}\int_0^{t-\varepsilon} vQd\tau dy = \int_{-R}^{R} k(x-y,\delta\varepsilon)\varphi(y,t-\varepsilon)dy - \int_{-R}^{R} k(x-y,\delta t)\varphi(y,0)dy.$$

Now we let ε go to zero and R go to infinity and obtain:

$$\begin{aligned}\int_{-\infty}^{\infty}\int_0^{t} vQd\tau dy &= \lim_{\varepsilon\to 0}\int_{-\infty}^{\infty} k(x-y,\delta\varepsilon)\varphi(y,t-\varepsilon)dy \\ &\quad -\int_{-\infty}^{\infty} k(x-y,\delta t)\varphi(y,0)dy. \end{aligned}\tag{4.29}$$

One of the basic properties of the fundamental solution of the heat equation, as for example shown in [Guen, 1988] is:

$$\lim_{(x,t)\to(x_0,0+)}\int_{-\infty}^{\infty} k(x-y,at)f(y)dy = f(x_0).$$

This property transforms (4.29) into:

$$\begin{aligned}\int_{-\infty}^{\infty}\int_0^t vQ\,d\tau dy &= \lim_{(x,\varepsilon)\to(x,0)}\int_{-\infty}^{\infty} k(x-y,\delta\varepsilon)\varphi(y,t-\varepsilon)dy \\ &\quad -\int_{-\infty}^{\infty} k(x-y,\delta t)\varphi(y,0)dy \\ &= \varphi(x,t)-\int_{-\infty}^{\infty} k(x-y,\delta t)\varphi(y,0)dy. \qquad (4.30)\end{aligned}$$

Therefore, using the definitions of v and Q, given in (4.26) and (4.24),respectively, we get:

$$\begin{aligned}\varphi(x,t) &= \int_{-\infty}^{\infty} k(x-y,\delta t)\varphi(y,0)dy \\ &\quad +\int_{-\infty}^{\infty}\int_0^t k(x-y,\delta(t-\tau))(-\eta\ln\varphi\varphi - c(t)\varphi)d\tau dy. \qquad (4.31)\end{aligned}$$

We now found an implicitly defined solution of equation (4.20). For this solution, we will now prove existence and uniqueness with the following theorem.

Theorem 4.1 *There exists a unique solution of*

$$\begin{aligned}\varphi(x,t) &= \int_{-\infty}^{\infty} k(x-y,\delta t)\varphi(y,0)dy \\ &\quad +\int_{-\infty}^{\infty}\int_0^t k(x-y,\delta(t-\tau))(-\eta\varphi(y,\tau)\ln\varphi(y,\tau))d\tau dy \\ &\quad +\int_{-\infty}^{\infty}\int_0^t k(x-y,\delta(t-\tau))(-c(\tau)\varphi(y,\tau))d\tau dy,\end{aligned}$$

where

$$k(x,t)=\frac{1}{\sqrt{4\pi t}}\exp\left(-\frac{x^2}{4t}\right).$$

Proof: The proof of this theorem is shown in Appendix A.

In order to illustrate these results, let us take the initial condition $u(x,0) = \sin x$ and graph several iterations. The graph of the first iteration $u_0(x,t)$ was shown in the last section as figure 17. The second and third iterations (u_1, u_2) are shown in figure 18 and figure 19, respectively. We did not compute further iterations since the difference between $u_1(x,t)$ and $u_2(x,t)$ is already very small, as shown in figure 20, which raises the expectation that $u_2(x,t)$ did already converge very well.

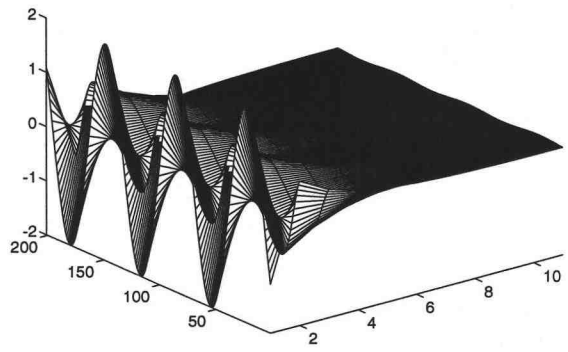

Figure 18. Second iteration: $u_1(x,t)$

In figure 19, we see that the solution smoothes out and does not lead to a rough surface.

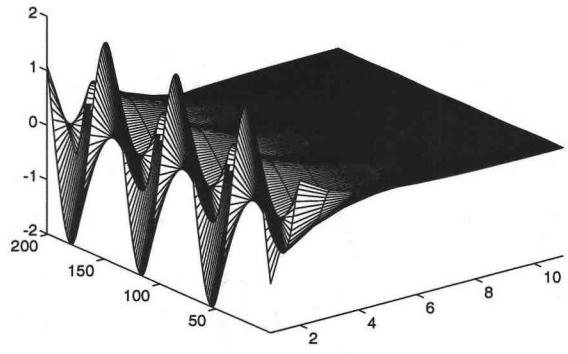

Figure 19. Third iteration: $u_2(x,t)$

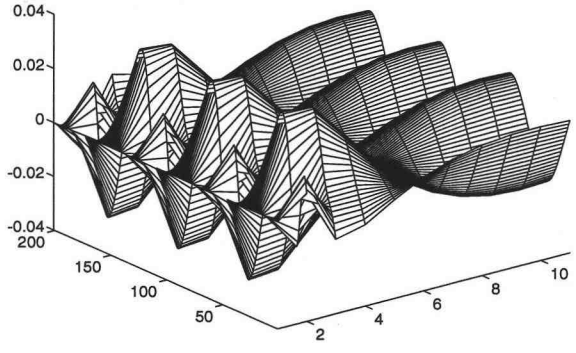

Figure 20. Difference between the second and the third iteration

4.5 Case e: $u_t + uu_x = \delta u_{xx}(1 + \varepsilon^2 u_x^2)^{-3/2}$

We shall first transform this equation into a conservation law. It is obvious that one can write the left hand side of the equation as $u_t + uu_x = (u)_t + (\frac{u^2}{2})_x$. It can be shown that the right hand side is equal to $\delta(u_x(1 + \varepsilon^2 u_x^2)^{-1/2})_x$. The equation in the form of a conservation law is

$$\frac{\partial}{\partial t}(u) = \frac{\partial}{\partial x}\left(\delta u_x(1 + \varepsilon^2 u_x^2)^{-1/2} - \frac{1}{2}u^2\right). \tag{4.32}$$

This cannot be solved analytically, but the following figure 21 shows a speculative numerical solution using *Fast Fourier transforms* and the *Runge-Kutta method.*

Using numerical methods, we will transform (4.32) into an equation, where the derivative of u with respect to t is equal to a function of u:

$$\frac{du}{dt} = f(u). \tag{4.33}$$

In order to find this function f, we will use *Fourier series* and *Fast Fourier transforms.* Note that we are considering periodic initial conditions. Hence, we can write u as a Fourier series with period L:

$$u(x) = \sum_{n=-\infty}^{\infty} a_n e^{i\mu_n x}, \tag{4.34}$$

where $\mu_n = 2\pi n L^{-1}$.

To find a numerical solution, we will need the discrete form of (4.34):

$$u_j = u(x_j) = \sum_{n=-\frac{1}{2}N}^{\frac{1}{2}N-1} a_n e^{i\mu_n x_j},$$

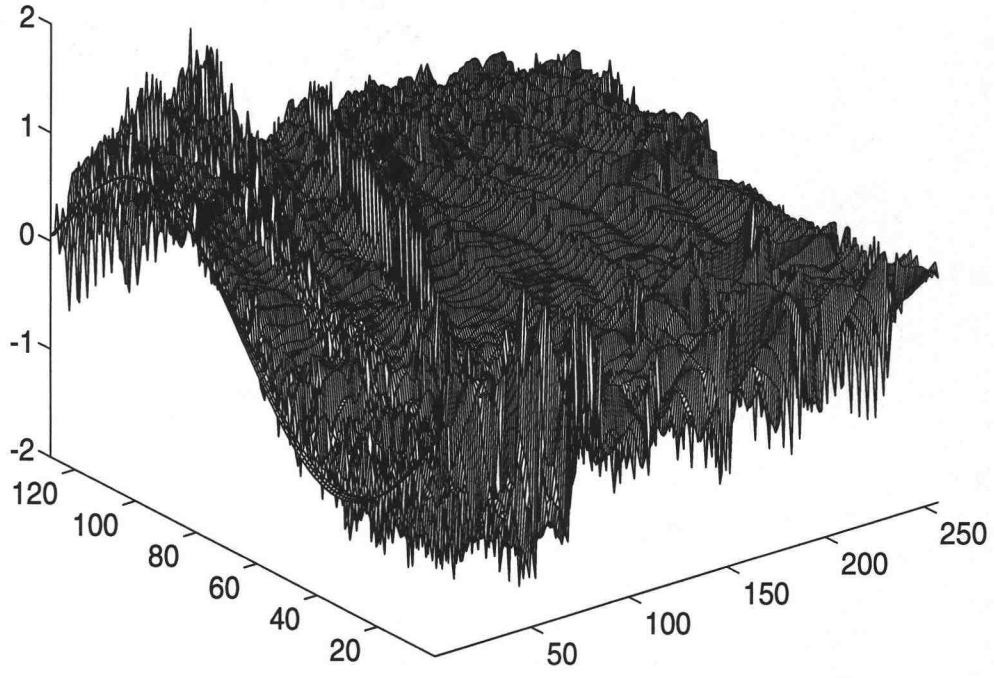

Figure 21. Speculative solution of $u_t + uu_x = \delta u_{xx}(1 + \varepsilon^2 u_x^2)^{-3/2}$

where $j = -\frac{1}{2}N, \ldots, \frac{1}{2}N - 1$.

Note: $\frac{1}{2}N$ is absent due to periodicity. Given the a_n's, the u_j's can be found using Fast Fourier transforms, and vice versa, given the u_j's, the a_n's can be computed with the inverse Fast Fourier transform. Therefore, we will be able to find the coefficients of the Fourier representation of our initial condition. These coefficients, on the other hand, will give us the derivative of u, which is:

$$u(x_j)' = \sum_{n=-\frac{1}{2}N+1}^{\frac{1}{2}N-1} (i\mu_n a_n) e^{i\mu_n x_j}.$$

Set $a_{-\frac{1}{2}N} = 0$, otherwise an unwanted imaginary component is introduced. The quantities $(i\mu_n a_n)$ are called *eigenvalues* of u. With this information, we found the quantity in parenthesis on the right hand side of (4.32). Set

$$v(x) = \delta u_x (1 + \varepsilon^2 u_x^2)^{-1/2} - \frac{1}{2}u^2.$$

To find the derivative of v with respect to x, we use the Fast Fourier transform again in order to obtain the coefficients of the Fourier series representation of v. As before, we can find the coefficients of the Fourier series representation of the derivative, and using the inverse Fast Fourier transform, we will find the actual derivative. Now, we transformed our problem into one of the form:

$$\frac{du}{dt} = f(u).$$

This form of our original equation can be solved numerically, using the *Runge Kutta method.*

Singularities in the solution to this equation develop quickly and are exacubated by

numerical inaccuracies. Consequently the Fourier transform becomes less trustworthy. The many singularities in the solution surface, however, indicate the physical behavior of the surface tension collapsing and a wave breaking open which in turn would enable water particles to leave the fluid body. This indicates that the surface shown in figure 21 does seem to represent the physical behavior of the onset of a breaking water surface. The onset of the roughness is being measured by the fact that the wave is tending toward being bounded by a fractal curve. A partial differential equation, however, may not be viewed as an appropriate tool to mathematically model breaking fluid surfaces and an alternate formulation is needed. It may be possible to introduce a suitable concept of a generalized solution to handle the case when singularities begin to appear, but such an appropriate concept is not clear at this time. We will therefore consider figure 21 as a *speculative solution*, showing a very rough surface behavior, which is what we expected to see in at least one of the cases of our wave equation.

4.6 Case f: $u_t + uu_x = \delta u_{xx}(1 + \varepsilon^2 u_x^2)^{-3/2} - \eta u$

This partial differential equation is the damped form of case e. Again we will not be able to solve it analytically, but using the same methods as in case e, we will obtain a numerical solution, which is shown in the following figure 22.

As expected, we note that the solution behaves more moderately than the one in figure 21, but it still shows a somewhat rough surface.

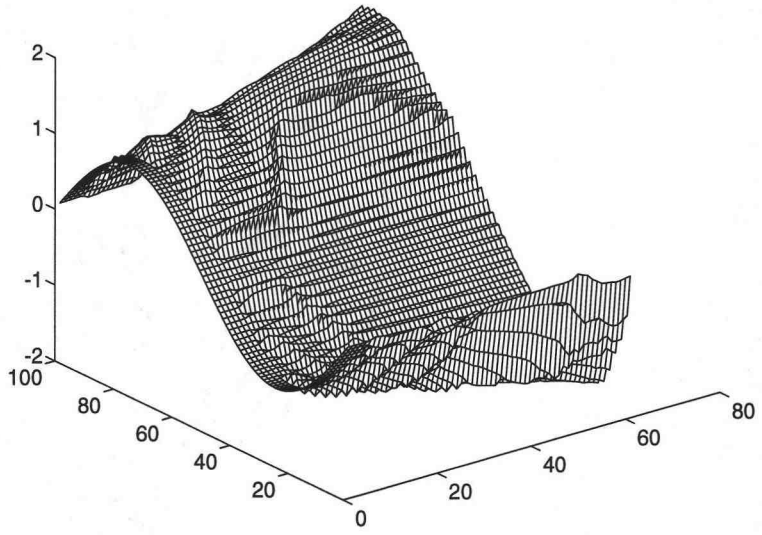

Figure 22. Solution of $u_t + uu_x = \delta u_{xx}(1 + \varepsilon^2 u_x^2)^{-3/2} - \eta u$

Chapter 5

Fractal Structure of Waves near their Breaking Point

In the preceding chapter, we found that in cases e and f of the wave equation, the wave surface starts to become very rough. In order to determine whether we have fractal surfaces, we will consider cross-sectional cuts of the wave at certain time steps. To measure the irregularity/roughness, we will use the box-counting method which was discussed in section 3.2.

Recall that, if we let F be a graph, then the box-counting dimension is defined to be

$$\dim_B(F) = \lim_{\delta \to 0} \frac{\log N_\delta(F)}{-\log \delta},$$

where $N_\delta(F)$ is, in our case, the smallest number of squares of length δ covering F. In order to find this limit, we use several grids of decreasing values of δ, count the boxes that cover F, respectively, and then fit a linear $(a + b\delta)$ and an exponential $(\exp(a + b\delta))$ model to these counts in order to predict the limit ($\delta = 0$). To justify the use of the box-counting method, we determined the dimensions of a linear, a

quadratic and a sine curve, which should be close to 1 if the box-counting method is valid. In the appendix, we show a table with the number of boxes covering F for different δ's, and the dimensions of the three different curves calculated according to the linear model fit. The exponential model was not found to fit the data significantly better than the linear model. Therefore the simpler (linear) model is used for predicting the dimensions. Using the linear model, we get the following dimensions:

- Linear curve: $1.10319 + 0.0130829\delta \Rightarrow \dim_B(F) \approx 1.10319$,
- Quadratic curve: $1.16182 + 0.0191629\delta \Rightarrow \dim_B(F) \approx 1.16182$,
- Sine curve: $1.14817 + 0.0215057\delta \Rightarrow \dim_B(F) \approx 1.14817$.

The true dimension in all three cases equals 1. The reason why the box-counting method does not achieve this value exactly is, that the measuring (counting) process is limited by a smallest box size greater than zero, at which the human eye cannot distinguish boxes any more. This creates a source of variation which leads to inaccurate dimensions.

The dimension of the surface shown in figure 21 is determined by taking cross-sectional cuts at time steps $M\ dt$, where dt is taken to be 0.02 and $M = 0$, 50, 100, 150, 200, 256. For $M = 0$ we get a sine curve, whose dimension is already known. The resulting dimensions according to the other time steps mentioned above are shown in the following table:

M	time step	$\dim_B(F)$
0	0	1.14817
50	1	1.42240
100	2	1.60361
150	3	1.56929
200	4	1.63834
256	5.12	1.64056

Table 1. Resulting dimensions for the time steps

We note that the dimensions for the curves corresponding to the surface at the time points $\neq 0$ above are significantly higher than the dimension for time $= 0$. This leads to the conclusion that these curves possess a fractal dimension in the plane. Moreover, the surface itself has a fractal dimension in space. In contrast, the dimension for an ocean wave and a wave in a wave tank was calculated to be 1.7 in [Gill, 1991].

BIBLIOGRAPHY

[Barn, 1988] Barnsley, M., *Fractals Everywhere*, San Diego: Academic Press, Inc., 1988.

[Baus, 1981] Bausch, R., V. Dohm, H.K. Janssen and R.K.P. Zia, *Critical Dynamics of an Interface in* $1+\varepsilon$ *Dimensions*, Physical Review Letters, 47 (1981), 1837-1840.

[Buff, 1965] Buff, F.P., R.A. Lovett and F.H. Stillinger, *Interfacial Density Profile for Fluid in the Critical Region*, Physical Review Letters, 15 (1965), 621-623.

[Dieh, 1980] Diehl, H.W., D.M. Kroll and H. Wagner, *The Interface in a Ginsburg-Landau-Wilson Model: Derivation of the Drumhead Model in the Low-Temperature Limit*, Zeitschrift für Physik B, 36 (1980), 329-333.

[Dusc, 1930] Duschek, A. and W. Mayer, *Lehrbuch der Differentialgeometrie, Bd. I*, Leipzig und Berlin: Verlag und Druck von B.G. Teubner, 1930.

[Falc, 1985] Falconer, K.J., *The Geometry of Fractal Sets*, Cambridge: Cambridge University Press, 1990.

[Falc, 1990] Falconer, K.J., *Fractal Geometry*, Chichester: John Wiley & Sons, 1990.

[Foll, 1984] Folland, G.B., *Real Analysis*, New York: John Wiley & Sons, 1984.

[Gill, 1991] Gilliland, C.L., *Waves and Fractals*, Masters Thesis, Oregon State University, 1991.

[Guen, 1988] Guenther, R.B. and J.W. Lee, *Partial Differential Equations of Mathematical Physics and Integral Equations*, Englewood Cliffs, New Jersey: Prentice-Hall, 1988.

[Hass, 1962] Hasselmann, K., *On the non-linear energy transfer in a gravity-wave spectrum*, Journal of Fluid Mechanics, 12 (1962), 481-500.

[Heno, 1976] Hénon, M., *A two-dimensional mapping with a strange attractor*, Communications in Mathematical Physics, 50 (1976), 69-77.

[Hopf, 1950] Hopf, E., *The Partial Differential Equation* $u_t + uu_x = \mu_{xx}$, Communications on Pure and Applied Mathematics, 3 (1950), 201-230.

[Kard, 1986] Kardar, M., G. Parisi and Y.-C. Zhang, *Dynamic Scaling of Growing Interfaces*, Physical Review Letters, 56 (1986), 889-892.

[Kard, 1987] Kardar, M. and Y.-C. Zhang, *Scaling of Directed Polymers in Random Media*, Physical Review Letters, 58 (1987), 2087-2090.

[Kawa, 1982-1] Kawasaki, K. and T. Ohta, *Kinetic Drumhead Model of Interface.I*, Progress of Theoretical Physics, 67 (1982), 147-163.

[Kawa, 1982-2] Kawasaki, K. and T. Ohta, *Kinetic Drumhead Model of Interface.II*, Progress of Theoretical Physics, 68 (1982), 129-147.

[Krug, 1991] Krug, J., *Die Entstehung fraktaler Oberflächen*, Thun Frankfurt am Main: Verlag Harri Deutsch, 1991.

[LeMe, 1991] Le Méhauté, A., *Fractal Geometries*, London: Penton Press, 1991.

[Lich, 1929] Lichtenstein, L., *Grundlagen der Hydromechanik*, Berlin: Verlag von Julius Springer, 1929.

[Mand, 1977a] Mandelbrot, B.B., *Fractals and turbulence: attractors and dispersion*, Lecture Notes in Mathematics, 615, (1977) .

[Mand, 1977b] Mandelbrot, B.B., *Fractals - Form, Chance, and Dimension*, San Francisco: W.H. Freeman and Company, 1977.

[Mand, 1983] Mandelbrot, B.B., *The Fractal Geometry of Nature*, New York: W.H. Freeman and Company, 1983.

[Medi, 1989] Medina, E., T. Hwa, M. Kardar and Y.-C. Zhang, *Burgers equation with correlated noise: Renormalization-group analysis and applications to directed polymers and interface growth*, Physical Review A, 39 (1989), 3053-3075.

[Oswa, 1959] Oswatitsch, K., *Physikalische Grundlagen der Strömungslehre, Handbuch der Physik, VIII/1*, Berlin Göttingen Heidelberg: Springer-Verlag, 1959.

[Peit, 1986] Peitgen, H.-O. and P.H. Richter, *The Beauty of Fractals*, Berlin Heidelberg: Springer-Verlag, 1986.

[Peit, 1988] Peitgen, H.-O. and D. Saupe (eds.), *The Science of Fractal Images*, New York: Springer-Verlag, 1988.

[Peit, 1992] Peitgen, H.-O., H. Jürgens and D. Saupe, *Chaos and Fractals*, New York: Springer-Verlag, 1992.

[Pier, 1955] Pierson, W.J., *Wind Generated Gravity Waves*, Advances in Geophysics vol.2, Academic Press Inc. Publishers New York, N. Y., (1955), 93-178.

[Serr, 1959] Serrin, J., *Mathematical Principles of Classical Fluid Mechanics*, Handbuch der Physik, VIII/1, Berlin Göttingen Heidelberg: Springer-Verlag, 1959.

[Stia, 1991] Stiassnie, M., *The Fractal Dimension of the Ocean Surface*, Nonlinear Topics of Ocean Physics, Proceedings of the International School of Physics Enrico Fermi, CIX, 633-647.

[Wall, 1979] Wallace, D.J. and R.K.P. Zia, *Euclidean Group as a Dynamical Symmetry of Surface Fluctuations: The Planar Interface and Critical Behavior*, Physical Review Letters, 43 (1979), 808-812.

[Weha, 1960] Wehausen, J.V. and E.V. Laitone, *Surface Waves*, Handbuch der Physik, IX, Berlin Göttingen Heidelberg: Springer-Verlag, 1960.

[Yosi, 1991] Yosida, K., *Lectures on Differential and Integral Equations*, New York: Dover Publications, Inc., 1991.

[Zakh, 1982] Zakharov, V.YE. and M.M. Zaslavskiy, *The Kinetic Equation and Kolmogorov Spectra in the Weak Turbulence Theory of Wind Waves*, Akademia Nauk SSSR, Atmospheric and Oceanic Physics, 18, pt.2 (1982), 747-753.

APPENDICES

Appendix A

Existence and Uniqueness Proof of Theorem 4.1

Theorem 4.1 *There exists a unique solution of*

$$\begin{aligned}\varphi(x,t) &= \int_{-\infty}^{\infty} k(x-y,\delta t)\varphi(y,0)dy \\ &\quad + \int_{-\infty}^{\infty}\int_{0}^{t} k(x-y,\delta(t-\tau))(-\eta\varphi(y,\tau)\ln\varphi(y,\tau))d\tau dy \\ &\quad + \int_{-\infty}^{\infty}\int_{0}^{t} k(x-y,\delta(t-\tau))(-c(\tau)\varphi(y,\tau))d\tau dy, \qquad \text{(A.1)}\end{aligned}$$

where

$$k(x,t) = \frac{1}{\sqrt{4\pi t}}\exp\left(-\frac{x^2}{4t}\right). \qquad \text{(A.2)}$$

Proof: For ease of notation, we will sometimes write k instead of $k(x-y,\delta(t-\tau))$. The initial condition $\varphi(x,0)$ equals $f(x)$. Set $\sup_y |f(y)| = M$. Since $\varphi(x,0) = \exp\{-\frac{1}{2\delta}\int u(x,0)dx\}$ and the initial condition for u is usually either a sine or a cosine function or a linear combination of both, we may assume that $\varphi(x,0)$ is bounded. Also set

$$\sup_t |c(t)| = C. \qquad \text{(A.3)}$$

EXISTENCE: Let us define a sequence of functions $\{\varphi_n(x,t)\}$ successively by:

$$\varphi_0(x,t) = \int_{-\infty}^{\infty} k(x-y,\delta t)f(y)dy \tag{A.4}$$

$$\begin{aligned}\varphi_1(x,t) &= \varphi_0(x,t) \\ &\quad + \int_{-\infty}^{\infty}\int_0^t k(x-y,\delta(t-\tau))(-\eta\varphi_0(y,\tau)\ln\varphi_0(y,\tau))d\tau dy \\ &\quad + \int_{-\infty}^{\infty}\int_0^t k(x-y,\delta(t-\tau))(-c(\tau)\varphi_0(y,\tau))d\tau dy \end{aligned} \tag{A.5}$$

$$\begin{aligned}\varphi_2(x,t) &= \varphi_0(x,t) \\ &\quad + \int_{-\infty}^{\infty}\int_0^t k(x-y,\delta(t-\tau))(-\eta\varphi_1(y,\tau)\ln\varphi_1(y,\tau))d\tau dy \\ &\quad + \int_{-\infty}^{\infty}\int_0^t k(x-y,\delta(t-\tau))(-c(\tau)\varphi_1(y,\tau))d\tau dy \\ &\vdots \\ \varphi_n(x,t) &= \varphi_0(x,t) \\ &\quad + \int_{-\infty}^{\infty}\int_0^t k(x-y,\delta(t-\tau))(-\eta\varphi_{n-1}(y,\tau)\ln\varphi_{n-1}(y,\tau))d\tau dy \\ &\quad + \int_{-\infty}^{\infty}\int_0^t k(x-y,\delta(t-\tau))(-c(\tau)\varphi_{n-1}(y,\tau))d\tau dy. \end{aligned}$$

Using the fact that $|f|$ has an upper bound and applying lemma 4.4 to equation (A.4), we find:

$$|\varphi_0(x,t)| \le M\int_{-\infty}^{\infty} k(x-y,\delta t)dy = M. \tag{A.6}$$

We have to prove now that $\{\varphi_n(x,t)\}$ converges uniformly, and the limit $\varphi(x,t)$ of the sequence $\{\varphi_n(x,t)\}$ is a solution of (A.1). For uniform convergence, we have

to show that $|\varphi_n(x,t) - \varphi_m(x,t)|$ tends to zero as n and m go to infinity. To obtain an expression for $|\varphi_n(x,t) - \varphi_m(x,t)|$, we will try to find upper bounds on $|\varphi_n(x,t) - \varphi_{n-1}(x,t)|$ for all n. Let $n = 1$, then:

$$\begin{aligned} |\varphi_1(x,t) - \varphi_0(x,t)| \leq & \int_{-\infty}^{\infty}\int_0^t |k(x-y,\delta(t-\tau))||\eta||\varphi_0(y,\tau)||\ln\varphi_0(y,\tau)|d\tau dy \\ & + \int_{-\infty}^{\infty}\int_0^t |k(x-y,\delta(t-\tau))||c(\tau)||\varphi_0(y,\tau)|d\tau dy. \end{aligned}$$

According to the bounds on φ_0 given in (A.6) and on $|c(\tau)|$ given in (A.3), we obtain:

$$\begin{aligned} |\varphi_1(x,t) - \varphi_0(x,t)| \leq & \int_{-\infty}^{\infty}\int_0^t |k(x-y,\delta(t-\tau))||\eta|M|\ln\varphi_0(y,\tau)|d\tau dy \\ & + \int_{-\infty}^{\infty}\int_0^t |k(x-y,\delta(t-\tau))|CMd\tau dy. \end{aligned}$$

Since $|\varphi_0| \leq M$, we can apply lemma 4.3 and therefore find the bound $\ln D$ for $\ln\varphi_0$. Now,

$$|\varphi_1(x,t) - \varphi_0(x,t)| \leq \int_0^t \left((|\eta|M\ln D + CM)\int_{-\infty}^{\infty} |k(x-y,\delta(t-\tau))|dy \right) d\tau.$$

Using lemma 4.4, we get:

$$\begin{aligned} |\varphi_1(x,t) - \varphi_0(x,t)| &\leq \int_0^t (|\eta|M\ln D + CM)d\tau \\ &= (|\eta|M\ln D + CM)t \\ &= M_1 t, \end{aligned} \tag{A.7}$$

where $M_1 = |\eta|M\ln D + CM$.

Let $n = 2$, then:

$$|\varphi_2(x,t) - \varphi_1(x,t)| = \left| \int_{-\infty}^{\infty}\int_0^t k(x-y,\delta(t-\tau))\eta\varphi_1(y,\tau)\ln\varphi_1(y,\tau)d\tau dy \right.$$

$$
\begin{aligned}
&- \int_{-\infty}^{\infty} \int_0^t k(x-y, \delta(t-\tau)) \eta \varphi_0(y,\tau) \ln \varphi_0(y,\tau) d\tau dy \\
&+ \int_{-\infty}^{\infty} \int_0^t k(x-y, \delta(t-\tau)) c(\tau) \varphi_1(y,\tau) d\tau dy \\
&- \int_{-\infty}^{\infty} \int_0^t k(x-y, \delta(t-\tau)) c(\tau) \varphi_0(y,\tau) d\tau dy \Big| .
\end{aligned}
$$

Applying the mean value theorem to $\varphi \ln \varphi$, we find:

$$
\begin{aligned}
|\varphi_2(x,t) - \varphi_1(x,t)| \;\leq\; & \int_{-\infty}^{\infty} \int_0^t |k||\eta||\varphi_{1,0}(y,\tau)||\ln \varphi_{11}(y,\tau) + 1| d\tau dy \\
& + \int_{-\infty}^{\infty} \int_0^t |k||c(\tau)||\varphi_{1,0}(y,\tau)| d\tau dy,
\end{aligned}
$$

where $\varphi_1(y,\tau) - \varphi_0(y,\tau) = \varphi_{1,0}(y,\tau)$ and $\varphi_{11} \in [\varphi_0, \varphi_1]$ for fixed y and τ.

The results found in inequality (A.7), the bound on $|c(\tau)|$ in (A.3) and the triangle inequality result in:

$$
\begin{aligned}
|\varphi_2(x,t) - \varphi_1(x,t)| \;\leq\; & \int_{-\infty}^{\infty} \int_0^t |k||\eta| M_1 \tau |\ln \varphi_{11}(y,\tau)| d\tau dy \\
& + \int_{-\infty}^{\infty} \int_0^t |k||\eta| M_1 \tau d\tau dy + \int_{-\infty}^{\infty} \int_0^t |k| C M_1 \tau d\tau dy.
\end{aligned}
$$

The inequality (A.6) assures that φ_0 is bounded. Therefore inequality (A.7) implies that φ_1 is also bounded. Assume $\varphi_1 > \varphi_0$ for fixed x, t, then $\varphi_{11} \leq \varphi_1$. Therefore φ_{11} is bounded. If $\varphi_1 < \varphi_0$, then $\varphi_{11} \leq \varphi_0$. We will get the same result, namely that φ_{11} is bounded. Hence we can apply lemma 4.3 and get:

$$
\begin{aligned}
|\varphi_2(x,t) - \varphi_1(x,t)| \;\leq\; & \int_{-\infty}^{\infty} \int_0^t |k(x-y, \delta(t-\tau))||\eta| M_1 \tau |\ln(D_1 \tau)| d\tau dy \\
& + \int_{-\infty}^{\infty} \int_0^t |k(x-y, \delta(t-\tau))||\eta| M_1 \tau d\tau dy \\
& + \int_{-\infty}^{\infty} \int_0^t |k(x-y, \delta(t-\tau))| C M_1 \tau d\tau dy.
\end{aligned}
$$

Changing the order of integration and applying lemma 4.4, we get:

$$|\varphi_2(x,t)-\varphi_1(x,t)| \leq \int_0^t |\eta| M_1 \tau |\ln(D_1\tau)| d\tau + \int_0^t (|\eta|+C) M_1 \tau d\tau.$$

The laws of the logarithm and the triangle inequality lead to the next estimate:

$$\begin{aligned} |\varphi_2(x,t)-\varphi_1(x,t)| \leq\ & |\eta| M_1 |\ln D_1| \int_0^t \tau d\tau + |\eta| M_1 \int_0^t |\ln \tau| \tau d\tau \\ & + M_1 (|\eta|+C) \int_0^t \tau d\tau. \end{aligned} \tag{A.8}$$

The first and the third integral in equation (A.8) can be easily solved. In order to solve the second integral, we will use lemma 4.2, which we stated earlier. This leads us to the following:

$$|\varphi_2(x,t)-\varphi_1(x,t)| \leq \frac{1}{2} M_1 \left(|\eta| |\ln D_1| + |\eta| + C\right) t^2 + \frac{1}{2} |\eta| M_1 \left(\frac{1}{2} + |\ln t|\right) t^2.$$

The absolute value of $\ln t$ has different functions as bounds, depending on t being larger or smaller than 1:

$$|\ln t| \leq \begin{cases} t & \text{if } t \geq 1 \\ t^{-1/2} & \text{if } t < 1. \end{cases} \tag{A.9}$$

This fact gives two different results for $|\varphi_2(x,t)-\varphi_1(x,t)|$:

<u>For $t \geq 1$:</u>

$$\begin{aligned} |\varphi_2(x,t)-\varphi_1(x,t)| &\leq \frac{1}{2} M_1 \left(|\eta| |\ln D_1| + |\eta| + \frac{1}{2}|\eta| + C\right) t^2 + \frac{1}{2} |\eta| M_1 t^3 \\ &= \frac{1}{2} M_1 \left(|\eta| |\ln D_1| + \frac{3}{2}|\eta| + C\right) t^2 + \frac{1}{2} |\eta| M_1 t^3 \\ &= \frac{1}{2} A t^2 + \frac{1}{2} B t^3, \end{aligned}$$

where $A = M_1\left(|\eta||\ln D_1| + \frac{3}{2}|\eta| + C\right)$ and $B = |\eta|M_1$.

Since $t^3 \geq t^2$ for all t greater than or equal to 1, we find:

$$\begin{aligned} |\varphi_2(x,t) - \varphi_1(x,t)| &\leq \frac{1}{2}(A+B)t^3 \\ &= \frac{1}{2}M_2 t^3, \end{aligned}$$

where $M_2 = A + B = M_1\left(|\eta||\ln D_1| + \frac{5}{2}|\eta| + C\right)$.

For $t < 1$:

$$\begin{aligned} |\varphi_2(x,t) - \varphi_1(x,t)| &\leq \frac{1}{2}M_1'\left(|\eta||\ln D_1| + |\eta| + \frac{1}{2}|\eta| + C\right)t^2 + \frac{1}{2}|\eta|M_1' t^{3/2} \\ &= \frac{1}{2}M_1'\left(|\eta||\ln D_1| + \frac{3}{2}|\eta| + C\right)t^2 + \frac{1}{2}|\eta|M_1' t^{3/2} \\ &= \frac{1}{2}At^{3/2} + \frac{1}{2}Bt^2, \end{aligned}$$

where $A = |\eta|M_1'$ and $B = M_1'\left(|\eta||\ln D_1| + \frac{3}{2}|\eta| + C\right)$.

Since $t^{3/2} \geq t^2$ for all t less than or equal to 1, we find:

$$\begin{aligned} |\varphi_2(x,t) - \varphi_1(x,t)| &\leq \frac{1}{2}(A+B)t^{3/2} \\ &= \frac{1}{2}M_2' t^{3/2}, \end{aligned}$$

where $M_2' = A + B = M_1'\left(|\eta||\ln D_1| + \frac{5}{2}|\eta| + C\right)$.

Therefore, we get:

$$|\varphi_2(x,t) - \varphi_1(x,t)| \leq \begin{cases} \frac{1}{2}M_1\left(|\eta||\ln D_1| + \frac{5}{2}|\eta| + C\right)t^3 & \text{if } t \geq 1 \\ \frac{1}{2}M_1'\left(|\eta||\ln D_1| + \frac{5}{2}|\eta| + C\right)t^{3/2} & \text{if } t < 1. \end{cases} \tag{A.10}$$

Now, we will prove the general claim.

Claim A.1 *For all $n > 0$, the absolute value of the difference of φ_n and φ_{n-1} will satisfy the following inequality:*

$$|\varphi_n(x,t) - \varphi_{n-1}(x,t)| \leq \begin{cases} \frac{1}{2^{n-1}(n-1)!} M_n t^{2n-1} & \text{if } t \geq 1 \\ \frac{2^{n-1}\,3!}{(n+2)!} M_n' t^{(n+1)/2} & \text{if } t < 1, \end{cases} \tag{A.11}$$

where $M_n = M_{n-1}\left(\left(2 + \frac{1}{2(n-1)}\right)|\eta| + |\eta|\ln(D_{n-1}) + C\right)$

and $M_n' = M_{n-1}'\left(\left(2 + \frac{2}{n+2}\right)|\eta| + |\eta|\ln(D_{n-1}) + C\right)$.

Proof: By induction. Let $n = 2$ in (A.11), and compare it to equation (A.10), then one realizes, that the claim is already proven for $n = 2$. We will assume that it holds for n. Then:

$$\begin{aligned} |\varphi_{n+1}(x,t) - \varphi_n(x,t)| \;=\; & \Big| \int_{-\infty}^{\infty}\int_0^t k\ \eta\ \varphi_n(y,\tau)\ \ln\varphi_n(y,\tau)\ d\tau dy \\ & - \int_{-\infty}^{\infty}\int_0^t k\ \eta\ \varphi_{n-1}(y,\tau)\ \ln\varphi_{n-1}(y,\tau)\ d\tau dy \\ & + \int_{-\infty}^{\infty}\int_0^t k\ c(\tau)\ \varphi_n(y,\tau)\ d\tau dy \\ & - \int_{-\infty}^{\infty}\int_0^t k\ c(\tau)\ \varphi_{n-1}(y,\tau)\ d\tau dy \Big|. \end{aligned}$$

Applying the mean value theorem to $\varphi\ln\varphi$, we find:

$$\begin{aligned} |\varphi_{n+1}(x,t) - \varphi_n(x,t)| \;\leq\; & \int_{-\infty}^{\infty}\int_0^t |k||\eta||\varphi_{n,n-1}(y,\tau)||\ln\varphi_{nn}(y,\tau) + 1| d\tau dy \\ & + \int_{-\infty}^{\infty}\int_0^t |k||c(\tau)||\varphi_{n,n-1}(y,\tau)| d\tau dy, \end{aligned}$$

where $\varphi_n(y,\tau) - \varphi_{n-1}(y,\tau) = \varphi_{n,n-1}(y,\tau)$ and $\varphi_{nn} \in [\varphi_{n-1}, \varphi_n]$ for fixed y and τ. The assumption that the claim holds for n, the bound on $|c(\tau)|$ in (A.3) and the triangle inequality lead us to the next result, where we will consider different cases

for $t \geq 1$ and for $t < 1$.

First let $\underline{t \geq 1}$:

$$\begin{aligned}|\varphi_{n+1}(x,t) - \varphi_n(x,t)| \;\leq\; & \int_{-\infty}^{\infty}\int_0^t |k||\eta| \,\frac{1}{2^{n-1}(n-1)!}\, M_n\tau^{2n-1}|\ln\varphi_{nn}(y,\tau)|d\tau dy \\ & + \int_{-\infty}^{\infty}\int_0^t |k||\eta| \,\frac{1}{2^{n-1}(n-1)!}\, M_n\tau^{2n-1} d\tau dy \\ & + \int_{-\infty}^{\infty}\int_0^t |k|C \,\frac{1}{2^{n-1}(n-1)!}\, M_n\tau^{2n-1} d\tau dy.\end{aligned}$$

Using the same reasoning as we used for the case of $n = 2$, we find that φ_{nn} is bounded. This implies that we can apply lemma 4.3 and get:

$$\begin{aligned}|\varphi_{n+1}(x,t) - \varphi_n(x,t)| \;\leq\; & \int_{-\infty}^{\infty}\int_0^t |k||\eta| \,\frac{1}{2^{n-1}(n-1)!}\, M_n\tau^{2n-1}|\ln(D_n\tau)|d\tau dy \\ & + \int_{-\infty}^{\infty}\int_0^t |k||\eta| \,\frac{1}{2^{n-1}(n-1)!}\, M_n\tau^{2n-1} d\tau dy \\ & + \int_{-\infty}^{\infty}\int_0^t |k|C \,\frac{1}{2^{n-1}(n-1)!}\, M_n\tau^{2n-1} d\tau dy.\end{aligned}$$

Changing the order of integration and applying lemma 4.4, we find:

$$\begin{aligned}|\varphi_{n+1}(x,t) - \varphi_n(x,t)| \;\leq\; & \int_0^t |\eta| \frac{1}{2^{n-1}(n-1)!} M_n\tau^{2n-1}|\ln(D_n\tau)|d\tau \\ & + \int_0^t |\eta| \frac{1}{2^{n-1}(n-1)!} M_n\tau^{2n-1} d\tau \\ & + \int_0^t C \frac{1}{2^{n-1}(n-1)!} M_n\tau^{2n-1} d\tau.\end{aligned}$$

The laws of logarithm and the triangle inequality lead to the next estimate:

$$\begin{aligned}|\varphi_{n+1}(x,t) - \varphi_n(x,t)| \;\leq\; & \frac{1}{2^{n-1}(n-1)!} M_n \left(|\ln(D_n)||\eta| + |\eta| + C\right) \int_0^t \tau^{2n-1} d\tau \\ & + \frac{1}{2^{n-1}(n-1)!} M_n|\eta| \int_0^t \tau^{2n-1}|\ln(\tau)|d\tau.\end{aligned}$$

In order to solve the last integral above, we will use lemma 4.2, which we stated earlier. The other integral can be integrated in a straightforward manner.

$$|\varphi_{n+1}(x,t)-\varphi_n(x,t)| \leq \frac{1}{2^{n-1}(n-1)!}M_n\left(|\ln(D_n)||\eta|+|\eta|+C\right)\frac{1}{2n}t^{2n} + \frac{1}{2^{n-1}(n-1)!}\,M_n\,|\eta|\,\frac{1}{2n}t^{2n}\left(\frac{1}{2n}+|\ln t|\right).$$

The inequality stated in (A.9) provides a bound on the logarithm function. Therefore, we obtain the following:

$$|\varphi_{n+1}(x,t)-\varphi_n(x,t)| \leq \frac{1}{2^{n-1}(n-1)!}M_n\left(|\ln(D_n)||\eta|+|\eta|+C+|\eta|\frac{1}{2n}\right)\frac{1}{2n}t^{2n} + \frac{1}{2^{n-1}(n-1)!}\,M_n\,|\eta|\,\frac{1}{2n}\,t^{2n+1}.$$

Since $t^{2n+1} \geq t^{2n}$ for $t \geq 1$, we get:

$$\begin{aligned}|\varphi_{n+1}(x,t)-\varphi_n(x,t)| &\leq \frac{1}{2^n(n)!}M_n\left(|\ln(D_n)||\eta|+|\eta|+C+|\eta|\frac{1}{2n}+|\eta|\right)t^{2n+1}\\ &= \frac{1}{2^n(n)!}M_n\left(\left(2+\frac{1}{2n}\right)|\eta|+|\eta||\ln(D_n)|+C\right)t^{2(n+1)-1}.\end{aligned}$$

Comparing this with the definition for M_{n+1} in claim A.1, we realize that we found:

$$|\varphi_{n+1}(x,t)-\varphi_n(x,t)| \leq \frac{1}{2^n(n)!}\,M_{n+1}\,t^{2(n+1)-1}.$$

This is exactly the expression we claimed to get for $|\varphi_{n+1}(x,t)-\varphi_n(x,t)|$, if $t \geq 1$.

We will now consider the case for $\underline{t<1:}$

$$|\varphi_{n+1}(x,t)-\varphi_n(x,t)| \leq \int_{-\infty}^{\infty}\int_0^t |k|\,|\eta|\,\frac{2^{n-1}\,3!}{(n+2)!}\,M_n'\,\tau^{(n+1)/2}|\ln\varphi_{nn}(y,\tau)|\,d\tau dy$$

$$+\int_{-\infty}^{\infty}\int_{0}^{t}|k|\,|\eta|\,\frac{2^{n-1}\,3!}{(n+2)!}\,M_n'\,\tau^{(n+1)/2}\,d\tau dy$$
$$+\int_{-\infty}^{\infty}\int_{0}^{t}|k|\,C\,\frac{2^{n-1}\,3!}{(n+2)!}\,M_n'\,\tau^{(n+1)/2}\,d\tau dy.$$

As before, φ_{nn} is bounded. Using lemma 4.3, we get:

$$\begin{aligned}|\varphi_{n+1}(x,t)-\varphi_n(x,t)| \;\leq\; & \int_{-\infty}^{\infty}\int_{0}^{t}|k|\,|\eta|\,\frac{2^{n-1}\,3!}{(n+2)!}\,M_n'\,\tau^{(n+1)/2}\,|\ln(D_n\tau)|\,d\tau dy\\ &+\int_{-\infty}^{\infty}\int_{0}^{t}|k|\,|\eta|\,\frac{2^{n-1}\,3!}{(n+2)!}\,M_n'\,\tau^{(n+1)/2}\,d\tau dy\\ &+\int_{-\infty}^{\infty}\int_{0}^{t}|k|\,C\,\frac{2^{n-1}\,3!}{(n+2)!}\,M_n'\,\tau^{(n+1)/2}\,d\tau dy.\end{aligned}$$

After changing the order of integration and applying lemma 4.4, we find:

$$\begin{aligned}|\varphi_{n+1}(x,t)-\varphi_n(x,t)| \;\leq\; & \int_{0}^{t}|\eta|\,\frac{2^{n-1}\,3!}{(n+2)!}\,M_n'\,\tau^{(n+1)/2}\,|\ln(D_n\tau)|\,d\tau\\ &+\int_{0}^{t}|\eta|\,\frac{2^{n-1}\,3!}{(n+2)!}\,M_n'\,\tau^{(n+1)/2}\,d\tau\\ &+\int_{0}^{t}C\,\frac{2^{n-1}\,3!}{(n+2)!}\,M_n'\,\tau^{(n+1)/2}\,d\tau.\end{aligned}$$

The next estimate follows from the laws of logarithm and the triangle inequality:

$$\begin{aligned}|\varphi_{n+1}(x,t)-\varphi_n(x,t)| \;\leq\; & \frac{2^{n-1}\,3!}{(n+2)!}\,M_n'\,(|\ln(D_n)||\eta|+|\eta|+C)\int_0^t\tau^{(n+1)/2}d\tau\\ &+\frac{2^{n-1}\,3!}{(n+2)!}\,M_n'\,|\eta|\int_0^t\tau^{(n+1)/2}\,|\ln(\tau)|\,d\tau.\end{aligned}$$

The solution of the last integral is given by lemma 4.2:

$$\begin{aligned}|\varphi_{n+1}(x,t)-\varphi_n(x,t)| \;\leq\; & \frac{2^{n-1}\,3!}{(n+2)!}\,M_n'\,(|\ln(D_n)||\eta|+|\eta|+C)\,\frac{2}{n+3}\,t^{(n+3)/2}\\ &+\frac{2^{n-1}\,3!}{(n+2)!}\,M_n'\,|\eta|\,\frac{2}{n+3}\,t^{(n+3)/2}\left(\frac{2}{n+3}+|\ln t|\right).\end{aligned}$$

Applying the inequality given in (A.9), we find the following estimate:

$$|\varphi_{n+1}(x,t)-\varphi_n(x,t)| \;\leq\; \frac{2^{n-1}3!}{(n+2)!}M_n'\left(|\ln(D_n)||\eta|+|\eta|+C+\frac{2\,|\eta|}{n+3}\right)\frac{2\,t^{(n+3)/2}}{n+3}$$

$$+\frac{2^{n-1}\ 3!}{(n+2)!}\ M_n^{'}\ |\eta|\ \frac{2}{n+3}\ t^{(n+2)/2}.$$

Since $t^{(n+2)/2} \geq t^{(n+3)/2}$ for $t < 1$, we get:

$$\begin{aligned} |\varphi_{n+1}(x,t) - \varphi_n(x,t)| &\leq \frac{2^n\ 3!}{(n+3)!} M_n^{'} \left(|\ln(D_n)||\eta| + 2|\eta| + C + \frac{2|\eta|}{n+3} \right) t^{(n+2)/2} \\ &= \frac{2^n\ 3!\ M_n^{'}}{(n+3)!} \left(\left(2 + \frac{2}{n+3} \right) |\eta| + |\eta \ln(D_n)| + C \right) t^{(n+2)/2}. \end{aligned}$$

Comparing the quantity in parentheses above with the definition of $M_{n+1}^{'}$ in claim A.1, we realize that:

$$|\varphi_{n+1}(x,t) - \varphi_n(x,t)| \leq \frac{1}{2^n} M_{n+1}^{'} t.$$

This is exactly the expression, we claimed to get for $|\varphi_{n+1}(x,t) - \varphi_n(x,t)|$, if $t < 1$.

Since we now found the bounds for $|\varphi_n - \varphi_{n-1}|$, we will address the problem to prove that $|\varphi_n - \varphi_m|$ tends to zero as n and m tend to infinity. For $n > m$, we obtain by the triangle inequality:

$$\begin{aligned} |\varphi_n(x,t) - \varphi_m(x,t)| &\leq |\varphi_n(x,t) - \varphi_{n-1}(x,t)| + |\varphi_{n-1}(x,t) - \varphi_{n-2}(x,t)| + \cdots \\ &\quad + |\varphi_{m+1}(x,t) - \varphi_m(x,t)| \\ &= \sum_{i=m+1}^{n} |\varphi_i(x,t) - \varphi_{i-1}(x,t)| \\ &\leq \sum_{i=m+1}^{\infty} |\varphi_i(x,t) - \varphi_{i-1}(x,t)|. \end{aligned}$$

In order to apply claim A.1, we need to consider the two cases:

Case 1: $\underline{t \geq 1}$:

$$|\varphi_n(x,t) - \varphi_m(x,t)| \leq \sum_{i=m+1}^{\infty} \frac{1}{2^{i-1}(i-1)!} M_i t^{2i-1}.$$

After factoring out all the common factors, we obtain:

$$|\varphi_n(x,t) - \varphi_m(x,t)| \leq \frac{1}{2^m (m)!}\, t^{2m+1} \sum_{j=0}^{\infty} \frac{(m)!}{2^j\ (m+j)!}\ M_{m+1+j}\ t^{2j}.$$

The right side of the last inequality tends to zero as $n, m \to \infty$, provided that the infinite sum converges.

Claim A.2

$$\sum_{j=0}^{\infty} \frac{(m)!}{2^j\ (m+j)!}\ M_{m+1+j}\ t^{2j} < \infty.$$

Proof: To show that the infinite series $\sum_{j=0}^{\infty} a_j$, where $a_j = \frac{(m)!}{2^j\ (m+j)!}\ M_{m+1+j}\ t^{2j}$, converges, we will use the *ratio test.* Consider:

$$\begin{aligned} \lim_{j\to\infty} \left|\frac{a_{j+1}}{a_j}\right| &= \lim_{j\to\infty} \left|\frac{(m)!\ M_{m+2+j}\ t^{2(j+1)}\ 2^j\ (m+j)!}{2^{j+1}\ (m+j+1)!\ (m)!\ M_{m+1+j}\ t^{2j}}\right| \\ &= \lim_{j\to\infty} \left|\frac{M_{m+2+j}\ t^2}{2\ M_{m+1+j}\ (m+j+1)}\right|. \end{aligned}$$

Applying the definition of M, stated in claim A.1, we get:

$$\begin{aligned} \lim_{j\to\infty} \left|\frac{a_{j+1}}{a_j}\right| &= \lim_{j\to\infty} \left|\frac{M_{m+1+j}\ \left(\left(2 + \frac{1}{2(m+1+j)}\right)|\eta| + |\eta \ln D_{m+1+j} + C\right)\ t^2}{2\ M_{m+1+j}\ (m+j+1)}\right| \\ &= \lim_{j\to\infty} \left|\frac{\left(\left(2 + \frac{1}{2(m+1+j)}\right)|\eta| + |\eta \ln D_{m+1+j} + C\right)\ t^2}{2\ (m+j+1)}\right| \\ &= 0. \end{aligned}$$

Since the limit is less than 1, the ratio test proves that claim A.2 is true.

We will now consider the case, where $t < 1$.

Case 2: $\underline{t < 1}$:

$$|\varphi_n(x,t) - \varphi_m(x,t)| \leq \sum_{i=m+1}^{\infty} \frac{2^{i-1}\ 3!}{(i+2)!} M_i^{'}\ t^{(i+1)2}.$$

Factoring out the common factors, we obtain:

$$|\varphi_n(x,t) - \varphi_m(x,t)| \leq \frac{2^m\ 3!}{(m+3)!} \sum_{j=0}^{\infty} \frac{2^j\ (m+3)!}{(m+j)!} M_{m+1+j}^{'} t^{j/2}.$$

Assuming that the infinite series converges, we can conclude that the right side of the inequality tends to zero as $n, m \to \infty$.

Claim A.3

$$\sum_{j=0}^{\infty} \frac{2^j\ (m+3)!}{(m+j)!} M_{m+1+j}^{'} t^{\frac{j}{2}} < \infty.$$

Proof: We will show the convergence of this sequence, using the *ratio test*:

$$\begin{aligned} \lim_{j\to\infty} \left| \frac{a_{j+1}}{a_j} \right| &= \lim_{j\to\infty} \left| \frac{2(j+1)\ (m+3)!\ M_{m+2+j}^{'}\ t^{(j+1)/2}\ (m+j)!}{(m+j+1)!\ 2^j\ (m+3)!\ M_{m+1+j}^{'}\ t^{j/2}} \right| \\ &= \lim_{j\to\infty} \left| \frac{2\ M_{m+2+j}^{'}\ t^{\frac{1}{2}}}{(m+j+1)\ M_{m+1+j}^{'}} \right|. \end{aligned}$$

Recall the definition of $M^{'}$, stated in claim A.1:

$$M_{m+2+j}^{'} = M_{m+1+j}^{'} \left(\left(2 + \frac{2}{m+4+j} \right) |\eta| + |\eta| |\ln(D_{m+1+j})| + C \right).$$

This leads to the following:

$$\begin{aligned}
\lim_{j\to\infty}\left|\frac{a_{j+1}}{a_j}\right| &= \lim_{j\to\infty}\left|\frac{2\,M'_{m+1+j}\left(\left(2+\frac{2}{m+4+j}\right)|\eta|+|\eta||\ln(D_{m+1+j})|+C\right)\,t^{1/2}}{(m+j+1)\,M'_{m+1+j}}\right| \\
&= \lim_{j\to\infty}\left|\frac{2\,t^{1/2}}{(m+j+1)}\left(\left(2+\frac{2}{m+4+j}\right)|\eta|+|\eta||\ln(D_{m+1+j})|+C\right)\right| \\
&= 0.
\end{aligned}$$

Since the right hand sides of case 1 and case 2 both tend to zero as $n, m \to \infty$, $\{\varphi_n(x,t)\}$ converges uniformly to a function $\varphi(x,t)$. Therefore $\varphi(x,t)$ is continuous. To prove that $\varphi(x,t)$ is a solution, we use the following fact: If the sequence of functions $\{\varphi_n(x,t)\}$ converges uniformly and $\varphi_n(x,t)$ is continuous in the given domain, then:

$$\lim_{n\to\infty}\int_{-\infty}^{\infty}\int_0^t \varphi_n(y,\tau)d\tau dy = \int_{-\infty}^{\infty}\int_0^t (\lim_{n\to\infty}\varphi_n(x,t))d\tau dy.$$

Hence we obtain:

$$\begin{aligned}
\varphi(x,t) &= \lim_{n\to\infty}\varphi_{n+1}(x,t) \\
&= \varphi_0(x,t) \\
&\quad + \lim_{n\to\infty}\int_{-\infty}^{\infty}\int_0^t k(x-y,\delta(t-\tau))(-\eta\varphi_n(y,\tau)\ln\varphi_n(y,\tau))d\tau dy \\
&\quad + \lim_{n\to\infty}\int_{-\infty}^{\infty}\int_0^t k(x-y,\delta(t-\tau))(-c(\tau)\varphi_n(y,\tau))d\tau dy \\
&= \varphi_0(x,t) \\
&\quad + \int_{-\infty}^{\infty}\int_0^t k(x-y,\delta(t-\tau))\lim_{n\to\infty}(-\eta\varphi_n(y,\tau)\ln\varphi_n(y,\tau))d\tau dy \\
&\quad + \int_{-\infty}^{\infty}\int_0^t k(x-y,\delta(t-\tau))\lim_{n\to\infty}(-c(\tau)\varphi_n(y,\tau))d\tau dy
\end{aligned}$$

$$
\begin{aligned}
&= \varphi_0(x,t) \\
&\quad + \int_{-\infty}^{\infty}\int_0^t k(x-y,\delta(t-\tau))(-\eta\varphi(y,\tau)\ln\varphi(y,\tau) - c(\tau)\varphi(y,\tau))d\tau dy \\
&= \int_{-\infty}^{\infty} k(x-y,\delta t)f(y)dy \\
&\quad + \int_{-\infty}^{\infty}\int_0^t k(x-y,\delta(t-\tau))(-\eta\varphi(y,\tau)\ln\varphi(y,\tau) - c(\tau)\varphi(y,\tau))d\tau dy.
\end{aligned}
$$

Therefore $\varphi(x,t)$ is a solution of (A.1).

UNIQUENESS: Assume there exist two solutions φ_1 and φ_2 of equation (A.1). If φ_1 and φ_2 satisfy equation (A.1), then they also satisfy equation (4.25) and we obtain:

$$
\begin{aligned}
\varphi_{1t} - \delta\varphi_{1xx} &= Q(x,t), \qquad \varphi_1(x,0) = f(x) \\
\varphi_{2t} - \delta\varphi_{2xx} &= Q(x,t), \qquad \varphi_2(x,0) = f(x).
\end{aligned}
$$

Subtracting these two equations, we need to solve the following problem:

$$
(\varphi_1 - \varphi_2)_t - \delta(\varphi_1 - \varphi_2)_{xx} = 0 \qquad \text{and} \qquad \varphi_1(x,0) - \varphi_2(x,0) = 0.
$$

Let $\psi = \varphi_1 - \varphi_2$, then:

$$
\psi_t - \delta\psi_{xx} = 0 \qquad \text{and} \qquad \psi(x,0) = 0. \tag{A.12}
$$

Equation (A.12) is the heat equation, which we solved already in section 4.3 and the solution is given by equation (4.19):

$$
\psi(x,t) = \frac{1}{\sqrt{4\delta\pi t}}\int_{-\infty}^{\infty} e^{-\frac{(x-y)^2}{4\delta t}}\psi(y,0)\,dy,
$$

where $\psi(x,0)$ is the initial condition. In our case the initial condition $\psi(x,0) = 0$. Since the integral of zero equals zero, we note that $|\psi(x,t)| \equiv 0$. This implies that $\varphi_1 \equiv \varphi_2$. Therefore equation (A.1) has a unique solution and the proof is complete. ■

Appendix B

Dimensions of a Linear, a Quadratic and a Sine Curve

B.1 Linear Curve

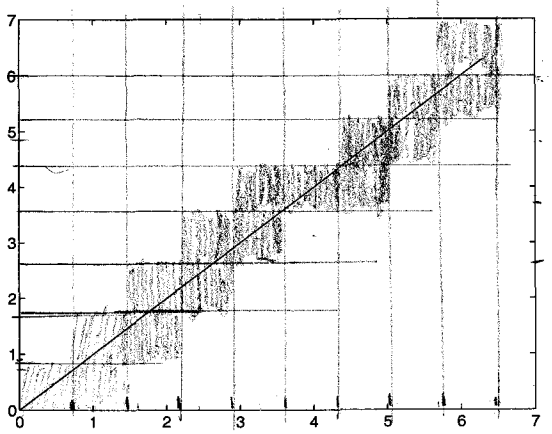

Figure 23. Linear curve

The linear fit program employed indicated that the best linear fit to our data obtained by counting boxes covered by the linear curve at various box lengths was $\dim_B(F) \approx 1.10319 + 0.0130829\delta$. Thus $\dim_B(F) = \lim_{\delta \to 0} \frac{\log N_\delta(F)}{-\log \delta} = 1.10319$.

LINEAR CURVE		
box dimension δ in dm	number of boxes N_δ	$-\ln N_\delta / \ln \delta$
.08	21	1.2054
.07	24	1.1951
.06	28	1.1844
.05	33	1.1672
.04	42	1.1612
.03	54	1.1376

Table 2. Box counts for the linear curve

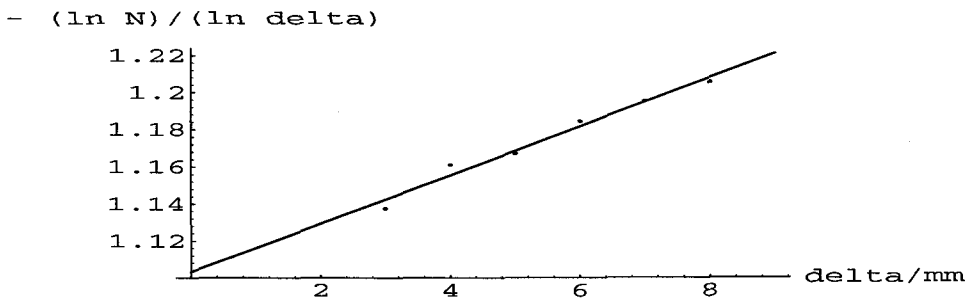

Figure 24. Linear fit and extrapolation for the linear curve

B.2 Quadratic Curve

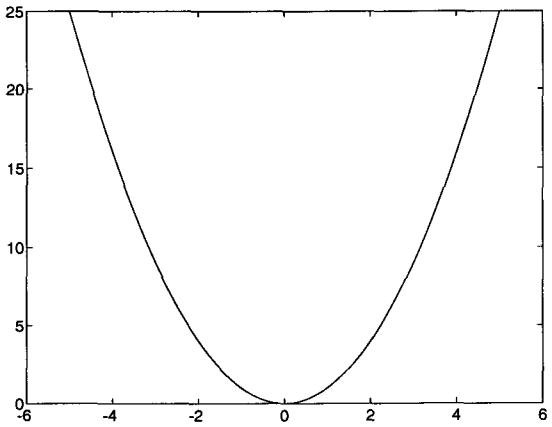

Figure 25. Quadratic curve

QUADRATIC CURVE		
box dimension δ in dm	number of boxes N_δ	$-\ln N_\delta / \ln \delta$
.08	28	1.3193
.07	30	1.2790
.06	37	1.2835
.05	45	1.2707
.04	54	1.2392
.03	70	1.2116

Table 3. Box counts for the quadratic curve

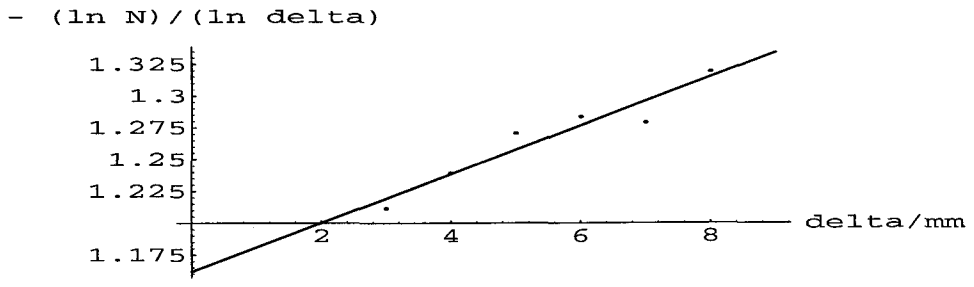

Figure 26. Linear fit and extrapolation for the quadratic curve

The linear fit program employed indicated that the best linear fit to our data obtained by counting boxes covered by the quadratic curve at various box lengths was $\dim_B(F) \approx 1.16182 + 0.0191629\delta$. Thus $\dim_B(F) = \lim_{\delta \to 0} \frac{\log N_\delta(F)}{-\log \delta} = 1.16182$.

B.3 Sine curve

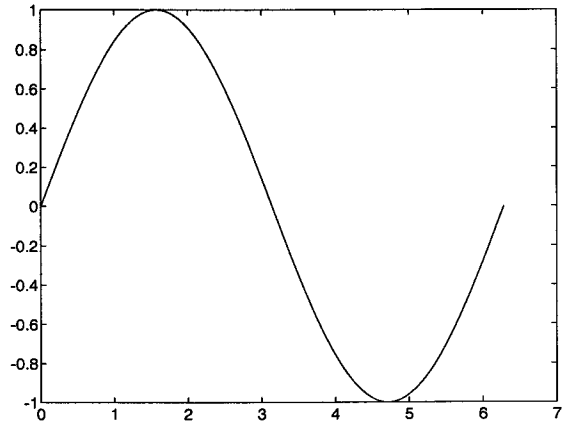

Figure 27. Sine curve

SINE CURVE		
box dimension δ in dm	number of boxes N_δ	$-\ln N_\delta / \ln \delta$
.08	27	1.3049
.07	32	1.3033
.06	38	1.2929
.05	45	1.2707
.04	50	1.2153
.03	70	1.2116

Table 4. Box counts for the sine curve

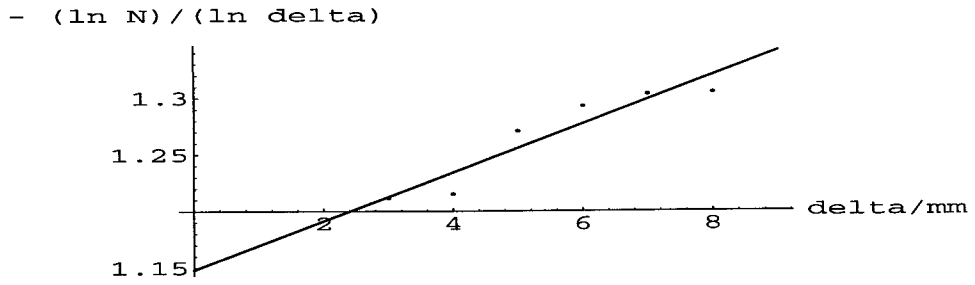

Figure 28. Linear fit and extrapolation for the sine curve

The linear fit program employed indicated that the best linear fit to our data obtained by counting boxes covered by the sine curve at various box lengths was $\dim_B(F) \approx 1.14817 + 0.02150576\delta$. Thus $\dim_B(F) = \lim_{\delta \to 0} \frac{\log N_\delta(F)}{-\log \delta} = 1.14817$.

Appendix C

Dimensions of Cross-Sectional Cuts at Certain Time Periods

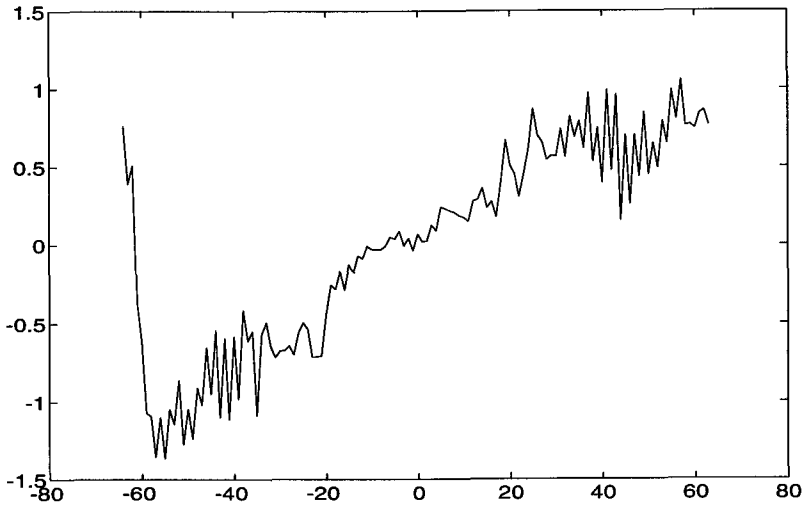

Figure 29. Cross-sectional cut at M = 50

The linear fit program employed indicated that the best linear fit to our data obtained by counting boxes covered by the curve shown in figure 29 at various box lengths was $\dim_B(F) \approx 1.42240 + 0.0141143\delta$. Thus $\dim_B(F) = \lim_{\delta \to 0} \frac{\log N_\delta(F)}{-\log \delta} = 1.42240$.

CROSS-SECTIONAL CUT AT M = 50		
box dimension δ in dm	number of boxes N_δ	$-\ln N_\delta / \ln \delta$
.08	47	1.5243
.07	60	1.5397
.06	70	1.5101
.05	86	1.4869
.04	111	1.4631
.03	177	1.4761

Table 5. Box counts for the cut at M = 50

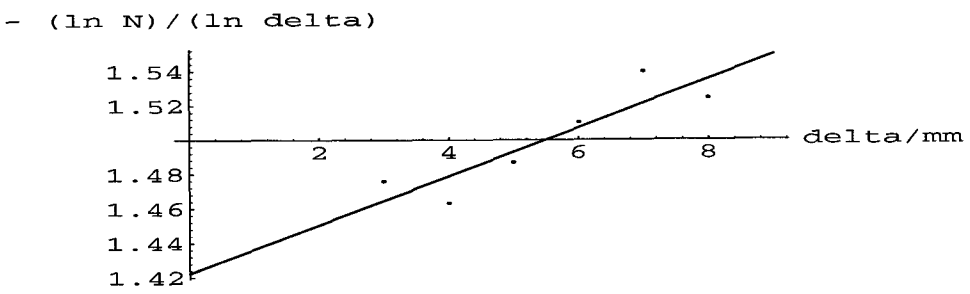

Figure 30. Linear fit and extrapolation for the cut at M = 50

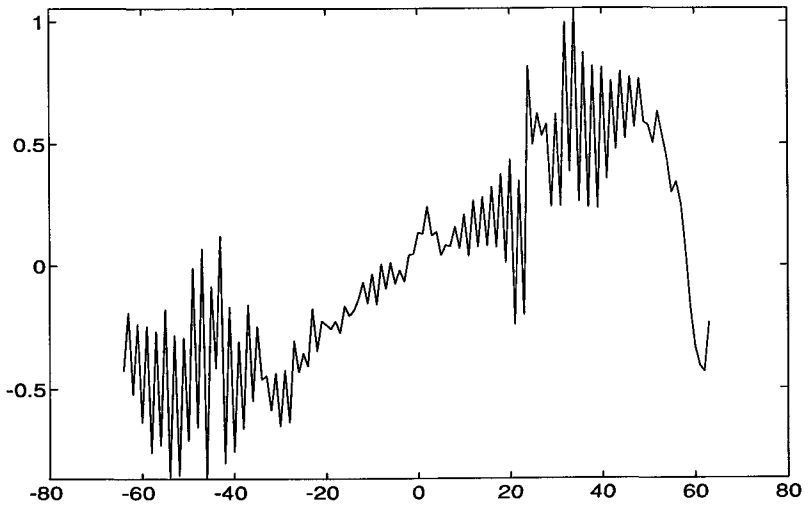

Figure 31. Cross-sectional cut at M = 100

CROSS-SECTIONAL CUT AT M = 100		
box dimension δ in dm	number of boxes N_δ	$-\ln N_\delta / \ln \delta$
.08	66	1.6588
.07	82	1.6571
.06	101	1.6404
.05	134	1.6349
.04	192	1.6333
.03	299	1.6257

Table 6. Box counts for the cut at M = 100

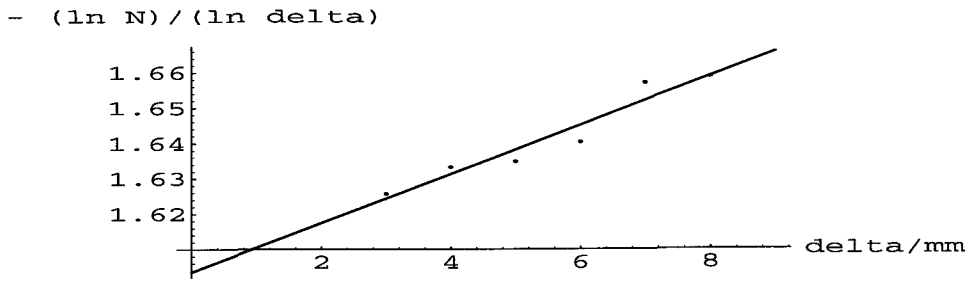

Figure 32. Linear fit and extrapolation for the cut at M = 100

The linear fit programm employed indicated that the best linear fit to our data obtained by counting boxes covered by the curve shown in figure 31 at various box lengths was $\dim_B(F) \approx 1.60361 + 0.006925715$. Thus $\dim_B(F) = \lim_{\delta \to 0} \frac{\log N_\delta(F)}{-\log \delta} =$ 1.60361.

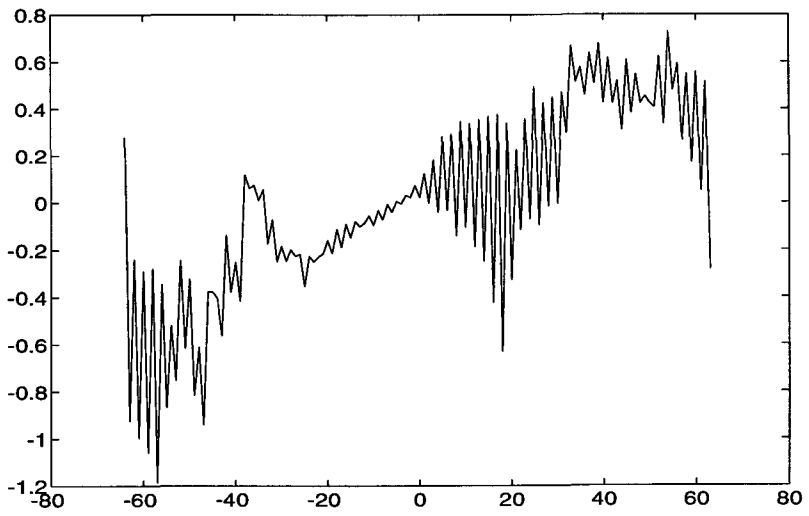

Figure 33. Cross-sectional cut at M = 150

CROSS-SECTIONAL CUT AT M = 150		
box dimension δ in dm	number of boxes N_δ	$-\ln N_\delta / \ln \delta$
.08	68	1.6706
.07	78	1.6383
.06	98	1.6297
.05	127	1.6170
.04	189	1.6284
.03	274	1.6008

Table 7. Box counts for the cut at M = 150

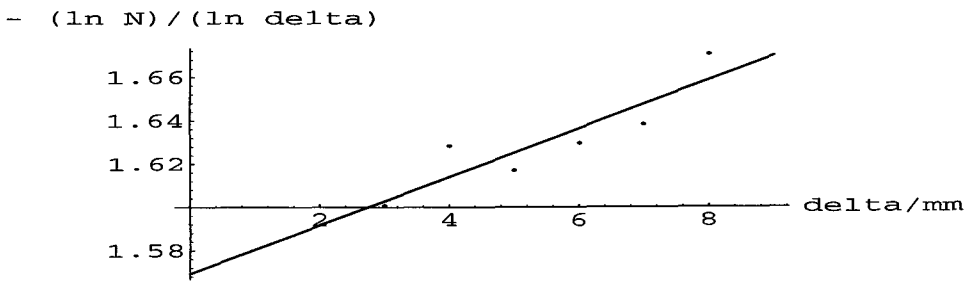

Figure 34. Linear fit and extrapolation for the cut at M = 150

The linear fit program employed indicated that the best linear fit to our data obtained by counting boxes covered by the curve shown in figure 33 at various box lengths was $\dim_B(F) \approx 1.56929 + 0.01118298$. Thus $\dim_B(F) = \lim_{\delta \to 0} \frac{\log N_\delta(F)}{-\log \delta} =$ 1.56929.

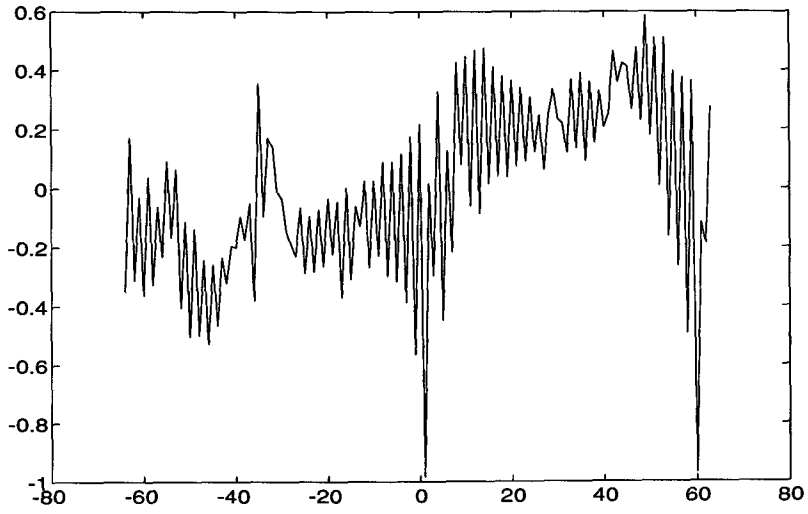

Figure 35. Cross-sectional cut at M = 200

CROSS-SECTIONAL CUT AT M = 200		
box dimension δ in dm	number of boxes N_δ	$-\ln N_\delta / \ln \delta$
.08	78	1.7249
.07	89	1.6879
.06	115	1.6865
.05	155	1.6835
.04	219	1.6742
.03	350	1.6706

Table 8. Box counts for the cut at M = 200

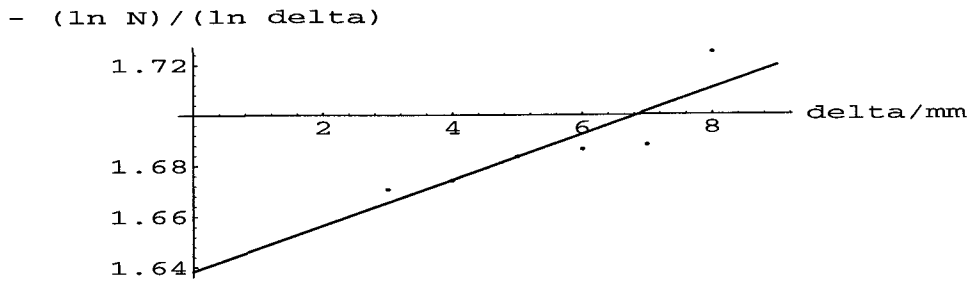

Figure 36. Linear fit and extrapolation for the cut at M = 200

The linear fit programm employed indicated that the best linear fit to our data obtained by counting boxes covered by the curve shown in figure 35 at various box lengths was $\dim_B(F) \approx 1.63834 + 0.009017148$. Thus $\dim_B(F) = \lim_{\delta \to 0} \frac{\log N_\delta(F)}{-\log \delta} =$ 1.63834.

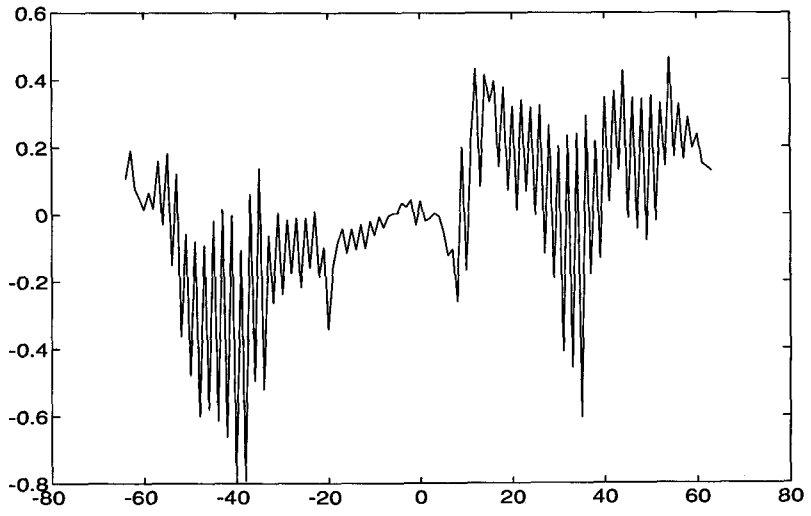

Figure 37. Cross-sectional cut at M = 256

CROSS-SECTIONAL CUT AT M = 256		
box dimension δ in dm	number of boxes N_δ	$-\ln N_\delta / \ln \delta$
.08	83	1.7495
.07	96	1.7165
.06	126	1.7190
.05	162	1.6983
.04	230	1.6894
.03	365	1.6825

Table 9. Box counts for the cut at M = 256

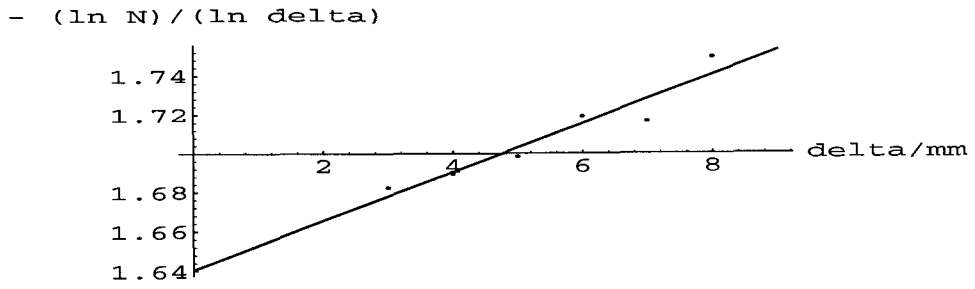

Figure 38. Linear fit and extrapolation for the cut at M = 256

The linear fit program employed indicated that the best linear fit to our data obtained by counting boxes covered by the curve shown in figure 37 at various box lengths was $\dim_B(F) \approx 1.64056 + 0.0124771\delta$. Thus $\dim_B(F) = \lim_{\delta \to 0} \frac{\log N_\delta(F)}{-\log \delta} =$ 1.64056.